



# A microtubule polymerase is required for microtubule orientation and dendrite pruning in *Drosophila*

Quan Tang<sup>1,2</sup> , Menglong Rui<sup>1,†</sup>, Shufeng Bu<sup>1,2,†</sup>, Yan Wang<sup>1</sup>, Liang Yuh Chew<sup>1,2</sup> & Fengwei Yu<sup>1,2,3,4,\*</sup> 

## Abstract

*Drosophila* class IV ddaC neurons selectively prune all larval dendrites to refine the nervous system during metamorphosis. During dendrite pruning, severing of proximal dendrites is preceded by local microtubule (MT) disassembly. Here, we identify an unexpected role of Mini spindles (Msps), a conserved MT polymerase, in governing dendrite pruning. Msps associates with another MT-associated protein TACC, and both stabilize each other in ddaC neurons. Moreover, Msps and TACC are required to orient minus-end-out MTs in dendrites. We further show that the functions of *msps* in dendritic MT orientation and dendrite pruning are antagonized by the kinesin-13 MT depolymerase Klp10A. Excessive MT depolymerization, which is induced by pharmacological treatment and katanin overexpression, also perturbs dendritic MT orientation and dendrite pruning, phenocopying *msps* mutants. Thus, we demonstrate that the MT polymerase Msps is required to form dendritic minus-end-out MTs and thereby promotes dendrite pruning in *Drosophila* sensory neurons.

**Keywords** dendrite; *Drosophila*; microtubule; minus-end-out orientation; pruning

**Subject Categories** Cell Adhesion, Polarity & Cytoskeleton; Neuroscience

**DOI** 10.15252/embj.2019103549 | Received 24 September 2019 | Revised 27 February 2020 | Accepted 28 February 2020 | Published online 8 April 2020

**The EMBO Journal (2020) 39: e103549**

## Introduction

Neurons often extend their exuberant processes and connections at early developmental stages. Selective removal of their unwanted or redundant dendrites or axons without causing neuronal death, referred to as pruning, is a fundamental strategy to ensure proper wiring in the developing nervous systems (Luo & O'Leary, 2005;

Riccomagno & Kolodkin, 2015; Schuldiner & Yaron, 2015). In mammalian brains, some developing neurons remove their long axonal bundles and re-establish functional circuits. Impaired neuronal pruning is associated with autism spectrum disorder (ASD) with increased dendritic spine density in layer V pyramidal neurons (Tang *et al.*, 2014). Neuronal pruning is also essential for the development of invertebrate nervous systems. In *Drosophila*, large-scale remodeling of nervous systems takes place during metamorphosis, a transition stage between larval and adult stages (Yu & Schuldiner, 2014; Kanamori *et al.*, 2015). Of interest, *Drosophila* dendritic arborization (da) neurons, which are part of the peripheral nervous system (PNS), undergo either apoptosis or pruning to generate adult-specific processes. Some dorsal dendrite arborization (dda) neurons (class I, ddaD and ddaE; class IV, ddaC or C4da) selectively prune away their larval dendrites but maintain their larval axons intact (Kuo *et al.*, 2005; Williams & Truman, 2005), whereas others (class III, ddaA and ddaF) are apoptotic during the first day of metamorphosis (Williams & Truman, 2005). Pruning involves blebbing, thinning, and retraction of neuronal branches, reminiscent of neurite degeneration associated with neurodegenerative diseases or spinal cord injury. Thus, developmental pruning might provide an important paradigm to unravel the mechanisms of neurodegeneration in pathological conditions.

*Drosophila* C4da or ddaC neurons have been established as a powerful system to understand the mechanisms of dendrite-specific pruning during early metamorphosis. Induced by a late larval pulse of the steroid hormone 20-hydroxyecdysone (ecdysone), ddaC neurons initially sever their larval dendrites at the proximal regions as early as 4 h after puparium formation (APF) and subsequently undergo rapid fragmentation and phagocyte-mediated debris clearance (Fig 1A; Williams & Truman, 2005; Han *et al.*, 2014). Upon the binding of ecdysone, a heterodimeric ecdysone receptor complex induces many downstream effectors or pathways. Among them are a transcription factor Sox14 (Kirilly *et al.*, 2009, 2011), a cytoskeletal regulator Mical (Kirilly *et al.*, 2009), Headcase (Loncle & Williams,

1 Temasek Life Sciences Laboratory, Singapore City, Singapore

2 Department of Biological Sciences, National University of Singapore, Singapore City, Singapore

3 NUS Graduate School for Integrative Sciences and Engineering, Centre for Life Sciences, Singapore City, Singapore

4 Neuroscience and Behavioral Disorder Program, Duke-NUS Graduate Medical School Singapore, Singapore City, Singapore

\*Corresponding author. Tel: +65 67827475; E-mail: fengwei@tll.org.sg

†These authors contributed equally to this work

2012), a Cullin1 E3 ligase complex (Wong *et al*, 2013), and calcium signaling (Kanamori *et al*, 2013). During pruning, microtubule (MT) disassembly precedes the scission of dendritic membrane in ddaC neurons (Williams & Truman, 2005). Three conventional MT-severing factors (namely katanin, spastin, and fidgetin) and multiple kinesin-13 MT depolymerases appear to be dispensable for dendrite pruning, as knockdown of these factors did not result in dendrite pruning defects in ddaC neurons (Lee *et al*, 2009; Stone *et al*, 2014; Tao *et al*, 2016). Katanin p60-like 1 (Kat-60L1), an AAA ATPase related to Katanin-60 (Kat-60) subunit, was reported to play a role in dendrite pruning of ddaC neurons (Lee *et al*, 2009), although its putative MT-severing function remains to be determined. Par-1 promotes MT breakdown probably via Tau inhibition and thereby dendrite pruning in ddaC neurons (Herzmann *et al*, 2017). However, despite the view that MT disassembly is a key step in the execution of dendrite pruning, the roles of MT polymerization/depolymerization factors in neuronal pruning remain poorly understood.

MTs are highly dynamic polymers formed by head-to-tail assembly of  $\alpha$ - and  $\beta$ -tubulin dimers. These intrinsically polarized structures contain two structurally distinct ends: a fast-growing plus end and a slow-growing minus end that exposes  $\beta$ -tubulins and  $\alpha$ -tubulins, respectively (Howard & Hyman, 2003; Akhmanova & Steinmetz, 2015). In contrast to static minus ends, plus ends are highly dynamic and can switch between phases of growth and shrinkage, a process known as “dynamic instability” (Howard & Hyman, 2003; Akhmanova & Steinmetz, 2015). Dynamic plus ends are decorated by MT plus-end tracking proteins (+TIPs) that promote MT dynamics (Akhmanova & Steinmetz, 2008). Highly conserved end-binding proteins (EBs) are the core components of the plus ends that provide a structural platform for recruiting other +TIPs (Honnappa *et al*, 2009). Neurons are highly polarized cells that extend two types of structurally and functionally distinct processes: a single long axon and multiple short dendrites. MTs are arranged with distinct orientations in axons and dendrites. In mammalian neurons, axons contain uniformly aligned MT arrays with their plus ends distal to the soma (plus-end-out), whereas dendrites are composed of MT bundles with a mixed orientation (Akhmanova & Steinmetz, 2015). In *Drosophila* and *C. elegans* neurons, MTs in axons are arranged with a plus-end-out orientation like those in mammalian counterparts (Baas *et al*, 1988; Stone *et al*, 2008; del Castillo *et al*, 2015). However, in dendrites, MTs are arranged with almost exclusive minus-end-out orientation in the major branches, although plus-end-out MTs are present in the terminal branches (Stone *et al*, 2008; Maniar *et al*, 2011; Goodwin *et al*, 2012; Ori-McKenney *et al*, 2012; Yalgin *et al*, 2015). *Caenorhabditis elegans* Unc-33 and *Drosophila*  $\gamma$ -tubulin were reported to regulate MT polarities in both axons and dendrites (Maniar *et al*, 2011; Nguyen *et al*, 2014). Plus-end-directed kinesin motor proteins, kinesin-1/2, mediate MT guidance or sliding to generate minus-end-out orientation of MT arrays in dendrites of *C. elegans* and *Drosophila* neurons (Mattie *et al*, 2010; Yan *et al*, 2013). *Kinesin-1/2* regulate dendrite pruning probably by aligning proper dendritic MT orientation in ddaC neurons (Herzmann *et al*, 2018). We and others have recently reported that the MT minus-end-binding protein Patronin, which also regulates uniform minus-end-out MT orientation in dendrites (Feng *et al*, 2019; Wang *et al*, 2019), is also critical for dendrite pruning (Wang *et al*, 2019). However, the molecular mechanism underlying the formation of dendritic MT orientation remains largely elusive.

Mini spindles (MSPs)/XMAP215/ch-TOG family proteins have been identified as key MT polymerases, which include Stu2/Dis1 in yeasts, Zyg9 in worms, MSPs in *Drosophila*, XMAP215 in *Xenopus*, and Ch-TOG in mammals (Al-Bassam & Chang, 2011). MSPs orthologs consist of multiple tumor-overexpressed gene (TOG) domains at the amino-terminus and a carboxyl-terminal domain (Al-Bassam & Chang, 2011). *In vitro* studies show that XMAP215 directly binds tubulin dimer via TOG domains to promote multiple rounds of tubulin addition as a MT polymerase (Brouhard *et al*, 2008). Loss of *Drosophila* MSPs or vertebrate XMAP215/ch-TOG leads to formation of small or aberrant spindle and short astral MTs during mitosis and meiosis (Cullen *et al*, 1999; Cullen & Ohkura, 2001; Gergely *et al*, 2003). MSPs family proteins can also function at MT-organizing centers (MTOCs) by directly interacting with transforming acidic coiled-coil (TACC) proteins via their carboxyl-terminal domains (Lee *et al*, 2001; Bellanger & Gonczy, 2003; Kinoshita *et al*, 2005). TACC proteins recruit MSPs/XMAP215 to centrosomes where they act together to assemble centrosomal MTs at the minus ends during mitosis (Cullen & Ohkura, 2001; Lee *et al*, 2001; Bellanger & Gonczy, 2003; Kinoshita *et al*, 2005). In postmitotic neurons, XMAP215 and ch-TOG promote MT growth by targeting to the tips of growing MTs in axons (van der Vaart *et al*, 2012; Lowery *et al*, 2013). Loss of XMAP215/ch-TOG leads to reduced MT growth rates and thereby impaired axon outgrowth in frog and rodent neurons. Vertebrate TACC proteins, which were initially identified as the centrosome-associated proteins in multiple organisms, colocalize with XMAP215/ch-TOG at MT plus ends and promote axonal outgrowth in cultured neurons (Nwagbara *et al*, 2014). However, the roles of MSPs and TACC in neuronal MT orientation and neuronal pruning have not been documented in invertebrates and vertebrates.

Here, we report the identification of MSPs as a novel regulator of dendrite pruning from a large-scale clonal screen. MSPs forms a protein complex with TACC in adult neurons, and both stabilize each other in ddaC neurons. Remarkably, we show that MSPs and TACC are required for minus-end-out MT orientation in dendrites of ddaC neurons, as impaired *mSPs* or *tacc* function resulted in a drastic decrease of the MT minus-end marker Nod- $\beta$ -gal and a significant increase of anterograde EB1-GFP comets in the major dendrites. Moreover, attenuation of the kinesin-13 MT depolymerase Klp10A significantly rescued dendrite pruning defects in *mSPs* RNAi ddaC neurons, suggesting that excessive MT depolymerization may result in dendritic MT orientation and dendrite pruning defects in mutant neurons. Consistent with this idea, MT depolymerization, which was induced by two MT-destabilizing drugs and Kat-60 overexpression, also led to formation of dendritic MTs with mixed orientations and dendrite pruning defects, resembling *mSPs* mutant phenotypes. Thus, our study demonstrates an important and unexpected role of the MT polymerase MSPs in regulating minus-end-out MT orientation in dendrites as well as dendrite pruning in *Drosophila* sensory neurons.

## Results

### MSPs is required for dendrite pruning of sensory neurons

To isolate novel players of dendrite pruning, we carried out a large-scale clonal screen on more than 3,000 mutagenized 3R

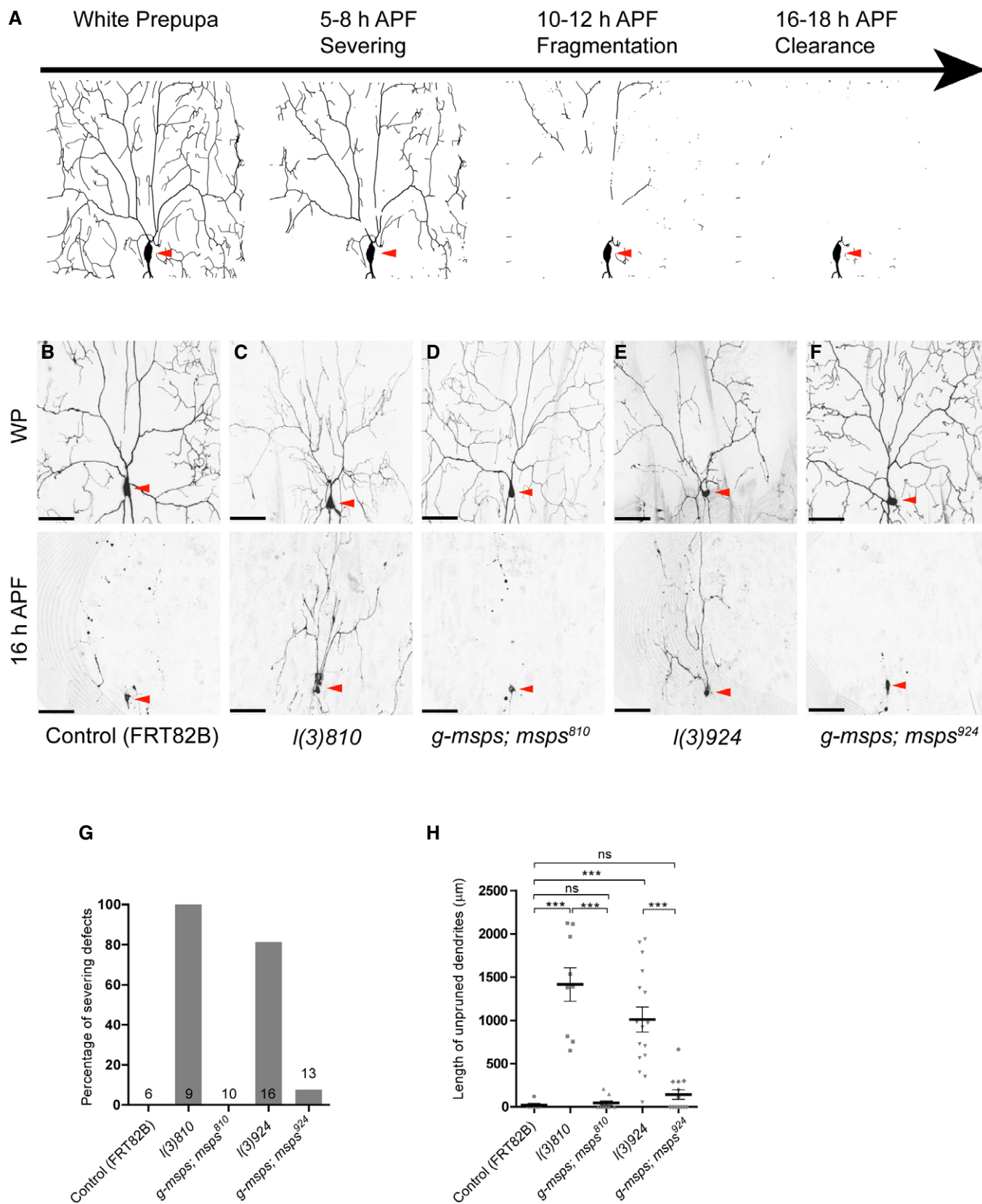


Figure 1.

**Figure 1. Msps is required for dendrite pruning in ddaC neurons.**

- A A schematic illustration of the dendrite pruning process in ddaC neurons. The time windows for three subdivided phases including severing, fragmentation, and clearance are listed. Red arrowheads point to the ddaC somas.
- B–F Live confocal images of ddaC clones expressing mCD8::GFP driven by *ppk-Gal4* at WP stage or 16 h APF. *l(3)810* and *l(3)924* mutant ddaC clones (C, E) displayed dendrite arborization defects at WP stage and pruning defects at 16 h APF. (D, F) Introduction of one genomic construct of *msps*, *HN267/g-msps*, rescued dendrite pruning defects in *msps<sup>810</sup>* and *msps<sup>924</sup>* clones. Red arrowheads point to the ddaC somas.
- G Percentages of ddaC clones showing severing defects at 16 h APF.
- H Quantitative analysis of unpruned dendrite lengths at 16 h APF.

Data information: In (G), the numbers above the bars represent the sample sizes. Error bars represent SEM from three independent experiments. Statistical significances were determined by one-way ANOVA with Bonferroni test, \*\*\* $P < 0.001$ , ns indicates statistically not significant. Scale bars represent 50  $\mu\text{m}$ .

Source data are available online for this figure.

chromosomes mutagenized by ethyl methanesulfonate (EMS). We induced homozygous mutant clones in a subset of dorsal class IV da (C4da or ddaC) neurons via the mosaic analysis with a repressible cell marker (MARCM) system (Lee & Luo, 2001). We isolated one complementation group containing two lethal mutants, *l(3)810* and *l(3)924*. Both alleles exhibited severe dendrite pruning defects in ddaC neurons at 16 h APF (Fig 1C and E). All *l(3)810* homozygous ddaC clones failed to sever their dendrites and retained an average of 1416  $\mu\text{m}$  dendrites in the vicinity of their soma (100%,  $n = 9$ ; Fig 1C, G and H). Likewise, the vast majority of *l(3)924* mutant neurons exhibited dendrite severing defects (81%,  $n = 16$ ; Fig 1E, G and H). By contrast, the wild-type neurons completely pruned their larval dendrites at the same time point ( $n = 6$ ; Fig 1B, G and H). In addition, simplified dendrite arbors were observed in either *l(3)810* or *l(3)924* at white prepupal (WP) stage (Fig 1C and E) as well as at larval stage (Appendix Fig S1A).

Like ddaC neurons, wild-type class I ddaD/E sensory neurons also completely pruned away their larval dendrites by 19 h APF (Appendix Fig S1B). *l(3)810* mutant ddaD/E neurons failed to prune their larval dendrites; as a result, some processes remained attached to their soma (67%,  $n = 3$ ; Appendix Fig S1B). Moreover, wild-type class III ddaF neurons were eliminated via apoptosis during early metamorphosis ( $n = 3$ ; Appendix Fig S1C). Similar to wild-type ones, mutant ddaF neurons homozygous for *l(3)810* died by 16 h APF ( $n = 3$ ; Appendix Fig S1C), suggesting that the *l(3)810*-associated mutation does not affect ddaF apoptosis.

To identify the molecular lesions of *l(3)810* and *l(3)924*, we performed deficiency mapping and complementation analysis with the existing lethal *P-element* insertion lines. We narrowed them down to the cytological region 89B1-B2, as both alleles failed to complement with *Df(3R)BSC728* and *Df(3R)Excel7328* deficiency lines (Fig EV1A). Moreover, both *l(3)810* and *l(3)924* alleles failed to complement with a lethal *P-element* line, *msps<sup>P</sup>* (Fig EV1B), which is inserted to the first intron of *msps* gene (Cullen *et al*, 1999). *Drosophila* Msps belongs to an evolutionarily conserved family of XMAP215/ch-TOG proteins that function as a key MT polymerase in animals, plants, and yeasts (Brouhard *et al*, 2008; Al-Bassam & Chang, 2011; Li *et al*, 2012). Subsequent DNA sequencing further revealed that *l(3)810* deletes a 47-nt fragment of the *msps* coding region and presumably generates a truncated Msps protein with the only N-terminal fragment aa1-535 (Fig EV1B). Moreover, immunostaining analyses reveal that Msps protein was undetectable in *msps<sup>810</sup>* mutant ddaC mutants ( $n = 4$ , Fig EV1C), suggesting that *l(3)810* is a null or strong hypomorphic allele of *msps*. Thus, we renamed *l(3)810* and *l(3)924* as *msps<sup>810</sup>* and *msps<sup>924</sup>*, respectively.

To genetically confirm that the phenotypes in *msps<sup>810</sup>* and *msps<sup>924</sup>* are caused by loss of *msps* function, we conducted two rescue experiments using an available transgene *HN267* carrying the *msps* genomic fragment (*g-msps*) (Fig EV1A; Cullen *et al*, 1999). This genomic fragment containing only *msps* gene was able to rescue both the lethality and dendrite pruning defects in *msps<sup>810</sup>* ( $n = 10$ ; Fig 1D, G and H) and *msps<sup>924</sup>* ( $n = 13$ ; Fig 1F–H) mutants. ddaC clones derived from *msps<sup>P18</sup>*, a hypomorphic allele, also exhibited dendrite pruning defects ( $n = 13$ ; Fig EV1D). Moreover, when *msps* was knocked down via two independent RNAi lines, similar dendrite arborization and pruning defects were observed in ddaC neurons at WP and 16 h APF, respectively (Fig EV1E). These larval dendrites were eventually pruned away at 32 h APF (Fig EV1F).

Taken together, Msps plays an important role in dendrite pruning in sensory neurons.

**Msps and TACC form a protein complex and stabilize each other in postmitotic neurons**

To investigate the molecular mechanism of Msps function, we next attempted to identify its binding partner that is also required for dendrite pruning. Msps and its vertebrate homologs were reported to interact with either TACC or  $\gamma$ -tubulin to regulate spindle formation and microtubule nucleation (Cullen & Ohkura, 2001; Lee *et al*, 2001; Gutierrez-Caballero *et al*, 2015; Thawani *et al*, 2018). To examine whether Msps forms a protein complex with TACC in postmitotic neurons, we conducted multiple sets of co-immunoprecipitation (co-IP) experiments using the protein extracts from adult brains. First, we co-overexpressed GFP-Msps and TACC in all adult neurons using the pan-neuronal driver *elav-Gal4*. In adult neurons, GFP-Msps formed a protein complex with TACC, as TACC was specifically detectable in the immune complex when GFP-Msps was immunoprecipitated from the protein extracts of adult brains using an anti-GFP antibody (Fig 2A). Reciprocally, endogenous Msps was also pulled down by overexpressed Venus-TACC in the co-IP experiments using adult brain extracts (Fig 2B). Furthermore, we conducted the co-IP assays using endogenous Msps and TACC proteins from adult brains. Endogenous Msps and TACC were co-immunoprecipitated in both directions (Fig 2C). As controls, no detectable  $\alpha$ -tubulin was pulled down in these co-IP assays (Fig 2A–C). These co-IP results demonstrate an *in vivo* association of Msps with TACC in adult neurons, suggesting that they may function together in neurons. We next defined which part of Msps is responsible for the association with TACC (Appendix Fig S2A). In S2 cell extracts, the C-terminal portion of Msps (Msps-C), rather than N-

terminal TOG domains (Msps-TOGs), is sufficient to co-immunoprecipitate with TACC (Appendix Fig S2A). Reciprocally, Msps-C was specifically pulled down by TACC (Appendix Fig S2A). These experiments indicate that the C-terminal fragment of Msps is essential to mediate its association with TACC, similar to their mammalian counterparts (Thakur *et al*, 2014). Interestingly, unlike its *Xenopus* counterpart (Thawani *et al*, 2018), Msps did not form a protein complex with  $\gamma$ -Tub23C, a major somatic  $\gamma$ -tubulin, in various co-IP experiments using the extracts from S2 cells (Appendix Fig S3A) or adult brains (Appendix Fig S3B).

We next examined whether Msps regulates the stability of TACC in ddaC sensory neurons or vice versa. TACC, which was abundantly expressed in the control RNAi neurons at wL3 stage ( $n = 33$ ; Fig 2D and H), was strongly reduced in *tacc* RNAi neurons ( $n = 16$ ; Fig 2F and H). Interestingly, in *msps* RNAi (#1) ddaC neurons, TACC levels were significantly reduced in their soma at wL3 stage ( $n = 13$ ; Fig 2E and H). Likewise, Msps expression, which was enriched in the control RNAi neurons ( $n = 28$ ; Fig 2I and M), was largely eliminated in the *msps* RNAi neurons ( $n = 10$ ; Fig 2J and M). Moreover, Msps levels also exhibited a significant decrease in the soma of ddaC neurons when TACC was knocked down ( $n = 15$ ; Fig 2K and M). Consistent with those in ddaC neurons, total TACC protein levels were strongly decreased in the larval brain extracts from *msps*<sup>810</sup>/*msps*<sup>P</sup> heterozygotes (Fig 2N). Total protein levels of Msps were also significantly reduced in the brain extracts from *tacc*<sup>59</sup>/*tacc*<sup>74</sup> transheterozygotes (Fig 2O). As a control, knockdown of  $\alpha$ -Tub84B, which led to a drastic reduction in overall MT density in ddaC neurons ( $n = 5$ ; Appendix Fig S2B), did not alter the protein levels of Msps and TACC in ddaC neurons ( $n = 7$  and 9, respectively; Fig 2G and L). These results suggest that the decrease in Msps or TACC protein levels is unlikely caused by reduced MT mass upon *tacc* or *msps* knockdown, respectively. In addition, the protein levels of Patronin were not affected in *msps* RNAi or *tacc* RNAi mutant neurons ( $n = 17$  and 24, respectively; Appendix Fig S2C). Thus, Msps and TACC are required to stabilize each other in postmitotic neurons including ddaC neurons.

### TACC is required for dendrite pruning in ddaC neurons

Since TACC binds and stabilizes Msps in neurons, we next investigated whether TACC, like Msps, is required for dendrite pruning. We made use of two independent RNAi lines targeting different *tacc* coding regions (#1, BL65982; #2, v101439). In contrast to no pruning defect in the control RNAi knockdown ( $n = 15$ , Fig 3A, D and E), knockdown of TACC, via one or two copies of *ppk-Gal4* driver led to similar pruning defects in ddaC neurons at 16 h APF (#1,  $n = 16$ , Fig 3B, D and E; #2,  $n = 25$ , Fig EV2A). ddaC neurons expressing *tacc* RNAi #1 or #2 lines failed to prune their larval dendrites (87 and 36%, respectively; Figs 3D and EV2A) and led to the persistence of their larval dendrites (Figs 3E and EV2A). Due to lack of null *tacc* mutants, we took advantage of the CRISPR/Cas9 technology to generate two large deletions, *tacc*<sup>59</sup> and *tacc*<sup>74</sup>, which uncover most of the *tacc* coding region (Fig EV2B). The vast majority of TACC protein was lost in the adult brains transheterozygous for *tacc*<sup>59</sup> and *tacc*<sup>74</sup> (Fig 2O). Thus, *tacc*<sup>59</sup> and *tacc*<sup>74</sup> are two null or strong hypomorphic *tacc* alleles. Importantly, ddaC neurons derived from *tacc*<sup>59</sup>/*tacc*<sup>74</sup> transheterozygotes exhibited simplified dendrite arbors at WP stage ( $n = 3$ , Fig EV2C) as well as dendrite pruning

defects at 16 h APF with full penetrance ( $n = 24$ , Fig 3C–E). The dendrite pruning defect is unlikely caused by developmental delay, as the transheterozygous animals exhibited normal head eversion and developed until adulthood. Thus, multiple lines of genetic data demonstrate that TACC, like Msps, plays an important role in regulating dendrite pruning.

To further determine whether Msps and TACC act in a common pathway or in two parallel pathways during dendrite pruning, we first double knocked down *msps* and *tacc* and compared with their single RNAi phenotypes. RNAi knockdown of *msps* with the control gene ( $n = 16$ ; Fig 3F, I and J) led to a stronger pruning phenotype than *tacc* RNAi plus control RNAi knockdown ( $n = 19$ ; Fig 3G, I and J). Importantly, no significant enhancement was observed in dendrite pruning defects in mutant ddaC neurons expressing both *msps* and *tacc* RNAi constructs ( $n = 16$ ; Fig 3H–J), compared to *msps* plus control RNAi knockdown ( $n = 16$ ; Fig 3F, I and J). Likewise, double MARCM ddaC clones of *msps*<sup>810</sup> and *tacc*<sup>59</sup> showed pruning defects to a similar extent as *msps*<sup>810</sup> single-mutant clones (Fig EV2D). These double-mutant analyses indicate no genetic interaction between *msps* and *tacc*. Thus, these results, together with the Msps-TACC association, suggest that Msps and TACC act in the same pathway to regulate dendrite pruning. In addition, MARCM ddaC clones derived from either  *$\gamma$ -tub23C*<sup>A15-2</sup> or  *$\gamma$ -tub23C*<sup>A14-9</sup> mutant did not exhibit any pruning defects ( $n = 14$  and 11, respectively; Appendix Fig S3C). Double knockdown of *msps* and  *$\gamma$ -tub23C* did not significantly enhance the pruning defects ( $n = 16$ ; Appendix Fig S3D), compared to those in *msps*, control RNAi neurons ( $n = 24$ ; Appendix Fig S3D). Thus, these data suggest that Msps acts to regulate dendrite pruning with TACC but independently of  $\gamma$ -tubulin in ddaC neurons.

### Msps and TACC are required for proper distribution of dendritic and axonal MT markers

Msps and TACC were reported to promote MT growth as a MT polymerase in mitotic cells and postmitotic neurons (Brouhard *et al*, 2008; van der Vaart *et al*, 2012; Lowery *et al*, 2013; Nwagbara *et al*, 2014). We first attempted to investigate whether Msps and TACC regulate overall MT levels in ddaC sensory neurons. Indeed, overall microtubules, which are detected by either the microtubule-associated protein Futsch (22C10) or  $\alpha$ -tubulin were significantly reduced in dendrites of *msps* RNAi ddaC neurons ( $n = 17$  and 11, respectively; Appendix Fig S4A and B), suggesting that Msps is required for overall MT mass in ddaC neurons. We next examined the distribution of two MT markers, namely Nod- $\beta$ -gal and Kin- $\beta$ -gal, in *msps* or *tacc* mutant neurons. The chimeric protein Nod- $\beta$ -gal, a marker of MT minus ends in *Drosophila* (Clark *et al*, 1997), is enriched in dendrites but not in axons in da sensory neurons (Rolls *et al*, 2007; Zheng *et al*, 2008). In wild-type ddaC neurons, Nod- $\beta$ -gal was specifically enriched in the dendrites and absent in the axons ( $n = 25$ , Fig 4A). Remarkably, Nod- $\beta$ -gal was highly concentrated in the soma with a drastic reduction in the dendrites of all *msps*<sup>810</sup> ( $n = 6$ ; Fig 4B and G) or *msps* RNAi ( $n = 12$ , Fig 4G) ddaC neurons. To quantify Nod- $\beta$ -gal alterations in dendrites, we measured its intensity in the major dendrite fragments that are 40  $\mu$ m away from the soma. In *msps*<sup>810</sup> (Fig 4H) or *msps* RNAi (Fig 4H) neurons, dendritic Nod- $\beta$ -gal levels were drastically reduced to 4 and 23% of that in the control neurons, respectively.

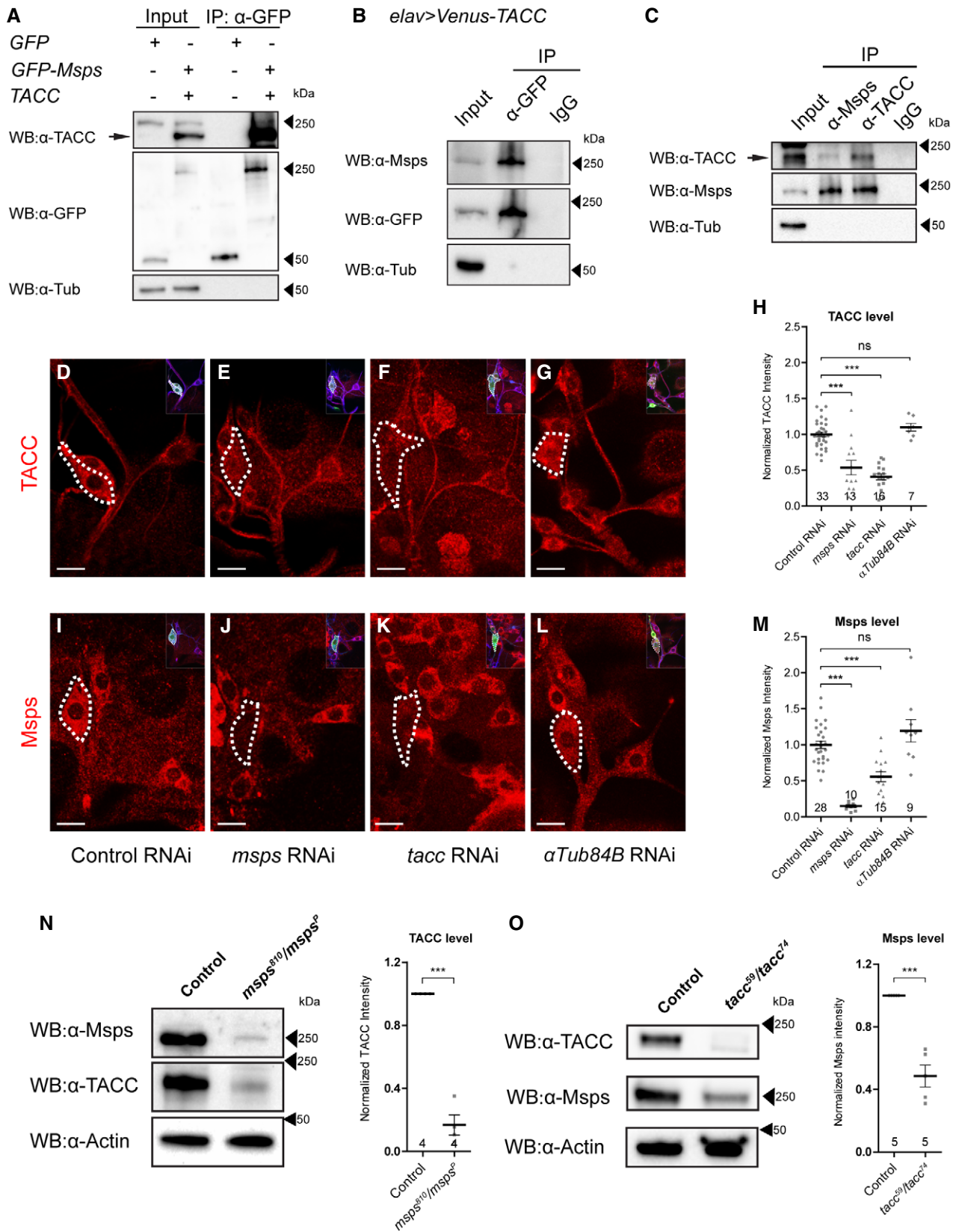


Figure 2.

**Figure 2. Msps and TACC associate and stabilize each other in postmitotic neurons..**

- A Pan-neuronal driver *elav-Gal4* was used to co-express GFP-Msps and TACC in postmitotic neurons. *elav-Gal4*-driven mCD8::GFP expression was used as a control. TACC was pulled down by GFP-Msps but not by mCD8::GFP. Alpha-tubulin was used as a loading and probing control. Neither mCD8::GFP nor GFP-Msps could pull down alpha-tubulin.
- B Endogenous Msps proteins were co-immunoprecipitated with Venus-TACC by GFP beads but not by control IgG beads. Alpha-tubulin was used as loading and probing control.
- C Endogenous Msps or TACC was pulled down by their respective antibodies, and the other protein was simultaneously detected in the immunoprecipitated contents. Alpha-tubulin was used as loading and probing control.
- D–G Confocal images of ddaC neurons expressing control RNAi (D), *msps* RNAi (E), *tacc* RNAi (F), and *α-Tub84B* RNAi (G) that were immunostained for TACC at wL3 stage. ddaC somas are labeled by dashed lines. ddaC neurons are identified by *ppk-Gal4*-driven mCD8::GFP (green channel) expression, as shown at the top right corner.
- H Quantitative analysis of normalized TACC fluorescence intensity in ddaC somas.
- I–L Confocal images of ddaC neurons expressing control RNAi (I), *msps* RNAi (J), *tacc* RNAi (K), and *α-Tub84B* RNAi (L) that were immunostained for Msps at wL3 stage. ddaC somas are labeled by dashed lines. ddaC neurons are identified by *ppk-Gal4*-driven mCD8::GFP (green channel) expression, as shown at the top right corner.
- M Quantitative analysis of normalized Msps fluorescence intensity in ddaC somas.
- N, O Protein expression of Msps and TACC in brain tissues. Larval brains of *msps<sup>810</sup>/msps<sup>P</sup>* transheterozygotes at early wL3 stage were immunoblotted and probed with  $\alpha$ -Msps and  $\alpha$ -TACC antibody. Actin blotting was used as loading control. The dot plot on the right depicts the quantitative analysis of total TACC levels in control and *msps* transheterozygous larvae. (O) Adult brains of *tacc<sup>59</sup>/tacc<sup>74</sup>* transheterozygotes were immunoblotted and probed with  $\alpha$ -Msps and  $\alpha$ -TACC antibody. Actin blotting was used as loading and probing control. The dot plot on the right displays the quantitative analysis of total Msps level in control and *tacc* transheterozygotes.

Data information: The numbers above the x-axis represent the sample sizes. Error bars represent SEM from three independent experiments. In (H, M), statistical significances were determined by one-way ANOVA with Bonferroni test, \*\*\**P* < 0.001, ns indicates statistically not significant. In (N, O), statistical significance was determined by two-tailed Student's *t*-test, \*\*\**P* < 0.001. Scale bars in (D–G, I–L) represents 10  $\mu$ m.

Source data are available online for this figure.

Likewise, in all *tacc<sup>59</sup>/tacc<sup>74</sup>* (*n* = 14; Fig 4C, G and H) or *tacc* RNAi (*n* = 14, Fig 4G and H), Nod- $\beta$ -gal accumulated to their soma and/or proximal dendrites with significant reduction in the distal dendrites (36 and 50% of the control levels, respectively). As controls, we also examined the distributions of cellular markers, such as Golgi outpost marker (ManII-Venus) and mitochondrial marker (Mito-GFP). No aberrant accumulation of these two markers was observed in the soma of *msps* RNAi neurons (*n* = 8 and 11, respectively; Appendix Fig S4C). In the distal dendrites of *msps* or *tacc* RNAi neurons, mitochondria were reduced in number; however, more Golgi outposts were present (Appendix Fig S4D). Thus, drastic Nod- $\beta$ -gal accumulations in the soma with its reduced dendritic signals are unlikely caused by soma-to-dendrite traffic jam.

We next utilized the axon-specific marker Kin- $\beta$ -gal which previously served as a marker of MT plus ends (Clark *et al*, 1997). Kin- $\beta$ -gal localized exclusively in the axons, but was absent in the dendrites of wild-type ddaC neurons (*n* = 11; Fig 4D and I; Zheng *et al*, 2008). Remarkably, in *msps* RNAi or *tacc* RNAi ddaC neurons, Kin- $\beta$ -gal was mis-localized to the dendrites (83%, *n* = 12, Fig 4E and I; 71%, *n* = 24, Fig 4F and I, respectively). Due to an unknown mechanism, Kin-LacZ often accumulated as several big blobs in *msps* RNAi dendrites (Fig 4E), which is different from its uniform distribution in the axons.

Thus, the Msps-TACC complex is required for proper distribution of dendrite or axon-specific MT markers in ddaC neurons.

**The Msps-TACC complex is required for minus-end-out MT orientation in dendrites**

In ddaC neurons, microtubules (MTs) are oriented minus-end-out in dendrites but plus-end-out in axons (Stone *et al*, 2008). The mis-localization of Nod- $\beta$ -gal and Kin- $\beta$ -gal markers in *msps*-depleted dendrites prompted us to further determine MT orientation in dendrites using the MT plus-end marker EB1-GFP. EB1-GFP labels plus ends of growing MTs, and its comet direction reflects MT orientation in neurons (Stepanova *et al*, 2003). In the major dendrites of

wild-type ddaC neurons, EB1-GFP comets predominantly moved retrogradely toward the soma (97%, *n* = 18 neurons, 280 comets; Fig 5A and G). EB1-GFP comets were lost in the dendrites of *msps<sup>810</sup>/msps<sup>P</sup>* transheterozygous mutant neurons (*n* = 24 neurons; Fig 5B), consistent with its role of Msps/XMAP215 as a MT polymerase (Brouhard *et al*, 2008; Li *et al*, 2012). We then took advantage of *msps<sup>P18</sup>*, a weaker *msps* allele (Chen *et al*, 2016), to assess EB1-GFP signals. Indeed, *msps<sup>810</sup>/msps<sup>P18</sup>* transheterozygous ddaC neurons exhibited detectable EB1-GFP comets. Remarkably, anterograde EB1-GFP comets were significantly increased to 27% in the dendrites of *msps<sup>810</sup>/msps<sup>P18</sup>* neurons (*n* = 20 neurons, 220 comets; Fig 5C and G), compared to approximately 3% in the control neurons (Fig 5A and G). Similarly, anterograde EB1-GFP comets were significantly increased to 50 and 38% in the dendrites of *tacc* RNAi (*n* = 24 neurons, 325 comets, Fig 5E and G) and *tacc<sup>59</sup>/tacc<sup>74</sup>* (*n* = 24 neurons, 431 comets, Fig 5F and G) neurons. These results, together with Nod- $\beta$ -gal and Kin- $\beta$ -gal data, demonstrate that both Msps and TACC are required for MT minus-end-out polarity in the dendrites of ddaC neurons. Of note, the length of EB1-GFP comet track, as measured by the distance of persistent MTs, was significantly reduced in *msps<sup>810</sup>/msps<sup>P18</sup>* (Fig 5H), *tacc* RNAi (Fig 5H), or *tacc<sup>59</sup>/tacc<sup>74</sup>* transheterozygous (Fig 5H) ddaC neurons, compared to that in the control neurons (Fig 5H). The average number of EB1-GFP comets was reduced in *msps<sup>810</sup>/msps<sup>P18</sup>* ddaC neurons (Fig 5I), however, remained the same in *tacc* RNAi or *tacc<sup>59</sup>/tacc<sup>74</sup>* transheterozygous neurons (Fig 5I). The average velocity of EB1-GFP comets was reduced in *tacc* RNAi or *tacc<sup>59</sup>/tacc<sup>74</sup>* transheterozygous neurons (Fig 5J). The EB1-GFP comets in the dendrites of *msps<sup>810</sup>/msps<sup>P18</sup>* (Fig 5C) and *tacc<sup>59</sup>/tacc<sup>74</sup>* (Fig 5F) mutant neurons appeared to be dimmer than those in the controls (Fig 5A and D). In contrast, we did not observe any MT orientation defect in the dendrites of mutant ddaC neurons transheterozygous for  $\gamma$ -*tub23C<sup>A14-9</sup>* and  $\gamma$ -*tub23C<sup>A15-2</sup>* (*n* = 6 neurons, 58 comets; Appendix Fig S3E).

Previous studies show that cytoskeletal disassembly or alterations can cause a neuronal stress response that restores MT levels or dynamics via JNK signaling (Massaro *et al*, 2009; Xiong *et al*,

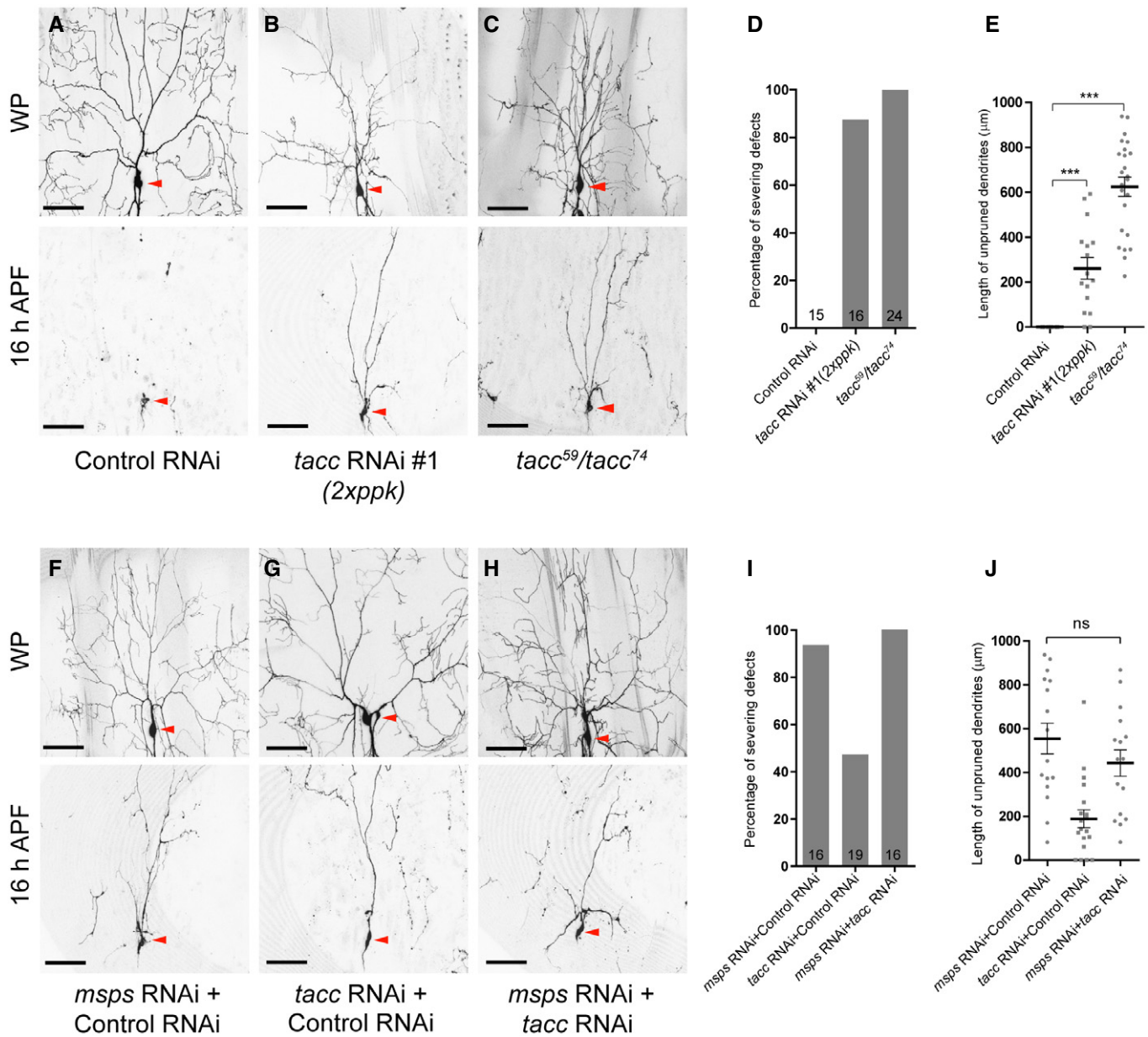


**Figure 3. *tacc* is required for dendrite pruning in *ddaC* neurons..**

A–C Live confocal images of *ddaC* neurons visualized by *ppk-Gal4*-driven *mCD8::GFP* expression at WP or 16 h APF. While expression of control RNAi in *ddaC* neurons (A) did not affect the dendrite morphogenesis nor the pruning processes, knockdown of *tacc* using RNAi #1 (B) or *tacc*<sup>59</sup>/*tacc*<sup>74</sup> transheterozygous mutant (C) severely perturbed the dendrite arborization as well as pruning. Red arrowheads point to the *ddaC* somas.

D Percentages of *ddaC* neurons showing severing defects in (A–C) at 16 h APF.

E Quantitative analysis of unpruned dendrite lengths in (A–C) at 16 h APF.

F–H Live confocal images of *ddaC* neurons visualized by *ppk-Gal4*-driven *mCD8::GFP* expression at WP or 16 h APF. Simultaneous knockdown of *tacc* and *mspis* via co-expressing *tacc* RNAi and *mspis* RNAi (H) in the *ddaC* neurons did not enhance the pruning defects, compared to those neurons co-expressing control RNAi and *mspis* RNAi (F). Red arrowheads point to the *ddaC* somas.

I Percentages of *ddaC* neurons showing severing defects in (F–H) at 16 h APF.

J Quantitative analysis of unpruned dendrite lengths in (F–H) at 16 h APF.

Data information: In (D, I), the numbers above the bars represent the sample sizes. Error bars represent SEM from three independent experiments. Statistical significances were determined by one-way ANOVA with Bonferroni test, \*\*\**P* < 0.001, ns indicates statistically not significant. Scale bars represent 50 μm.

Source data are available online for this figure.



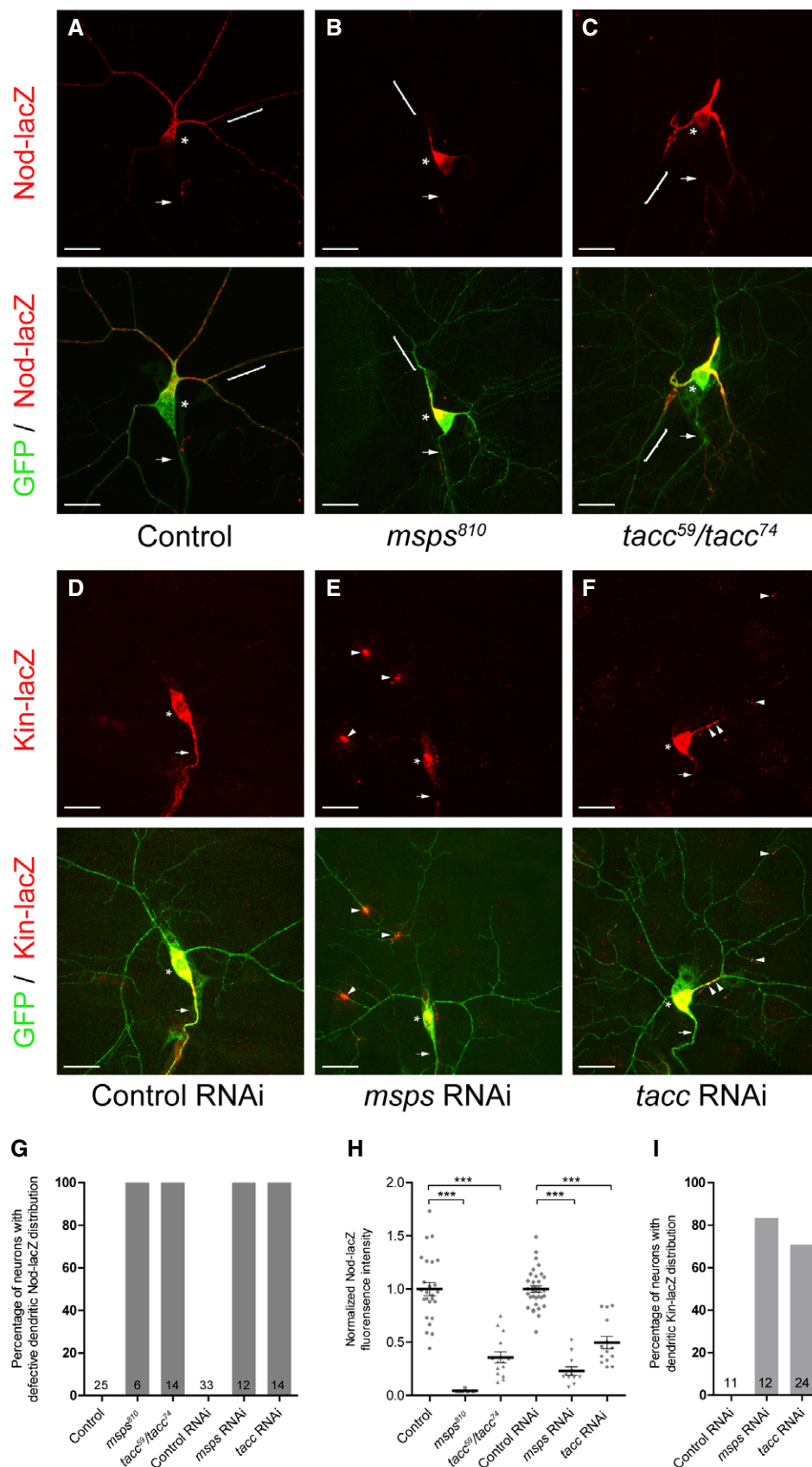


Figure 4.

**Figure 4. Msps and TACC are required for proper distribution of dendritic and axonal MT markers.**

- A–F Confocal images of ddaC neurons expressing *UAS-mCD8::GFP*, *UAS-Nod-lacZ*, or *UAS-Kin-lacZ* and immunostained for  $\beta$ -galactosidase at wL3 stages. (A–C) Wild-type ddaC neurons (A) displayed normal distribution of Nod-lacZ signals in dendrites. In contrast, in *msps*<sup>810</sup> mutants (B) and *tacc*<sup>59</sup>/*tacc*<sup>74</sup> mutants (C), ddaC neurons exhibited altered Nod-lacZ distribution patterns, with highly enriched stainings in the somas and decreased signals in the dendrites. (D–F) Kin-lacZ signals were present in axons but not detectable in dendrites of the control ddaC neurons (D), whereas part of the Kin-lacZ were mis-localized to dendrites in *msps* RNAi (E) and *tacc* RNAi (F) ddaC neurons. Asterisks indicate the location of ddaC somas. White arrows indicate the location of axons. Curly brackets mark the dendritic regions where fluorescence intensity of Nod-lacZ was measured. White arrowheads point to dendritically localized Kin-lacZ signals.
- G Percentages of ddaC neurons showing defective Nod-lacZ distribution in mutants or RNAi-expressing neurons.
- H Quantitative analysis of normalized Nod-lacZ intensity for 20  $\mu$ m of major dendrite located 40  $\mu$ m away from the soma.
- I Percentages of ddaC neurons showing defective Kin-lacZ distribution.

Data information: In (G, H, I), the numbers above the bars represent the sample sizes. Error bars represent SEM from three independent experiments. Statistical significances were determined by one-way ANOVA with Bonferroni test, \*\*\**P* < 0.001. Scale bars represent 20  $\mu$ m.

Source data are available online for this figure.

2010; Feng *et al.*, 2019). To investigate whether knockdown of *msps* or *tacc* causes the induction of JNK signaling, we utilized the *puc-lacZ* reporter to examine the level of JNK signaling in *msps* or *tacc* RNAi ddaC neurons. In the control ddaC neurons, *puc-lacZ* was expressed at a low level in their nuclei (*n* = 17, Fig EV3A; *n* = 19, Appendix Fig S5A). However, its expression levels were significantly increased when either *msps* (*n* = 18, Fig EV3A; *n* = 19, Appendix Fig S5A) or *tacc* (*n* = 18, Appendix Fig S5A) was knocked down. The *puc-lacZ* level in *msps* RNAi neurons was increased more drastically than that in *tacc* RNAi neurons (Appendix Fig S5A). We first inhibited the JNK pathway via the treatment with GNE-3511, a potent JNK inhibitor (Feng *et al.*, 2019). GNE-3511 treatment, which completely inhibited the induction of *puc-lacZ* (Fig EV3A), did not rescue the mixed MT orientation defect in *msps* RNAi (*n* = 15, Fig EV3B) or *tacc* RNAi (*n* = 14, Fig EV3C) ddaC neurons, as shown by either Nod- $\beta$ -gal distribution or EB1-GFP comet direction, respectively. The induction of JNK signaling could also be fully inhibited by the expression of JNK<sup>DN</sup>, the dominant-negative form of JNK that is encoded by *bsk* in *Drosophila*. JNK<sup>DN</sup> expression did not rescue the defect in Nod- $\beta$ -gal distribution in *msps* RNAi neurons (#1, *n* = 15; #2, *n* = 17; Appendix Fig S5B). Moreover, both GNE-3511 treatment and JNK<sup>DN</sup> expression did not rescue the dendrite pruning defects in *msps* RNAi neurons (*n* = 12, Fig EV3D; #1 and #2, *n* = 16 and 16, respectively; Appendix Fig S5C). Thus, Msps regulates dendritic MT orientation and dendrite pruning independently of JNK signaling.

Collectively, the Msps-TACC MT polymerase complex plays an important and JNK-independent role in regulating minus-end-out MT orientation in the dendrites of ddaC neurons.

### Msps function is antagonized by the kinesin-13 MT depolymerase Klp10A during dendrite pruning

Msps/XMAP215 family proteins localize at MT plus ends to mediate MT growth (Brouhard *et al.*, 2008; Al-Bassam & Chang, 2011), whereas kinesin-related MT depolymerases including *Drosophila* kinesin-13 Klp10A and its ortholog MCAK are targeted to MT plus ends by EB-1 and induce MT catastrophe at MT ends (Hunter *et al.*, 2003; Mennella *et al.*, 2005). An antagonism between Msps/XMAP210 and Klp10A/MCAK determines dynamic instability of MTs and spindle size in mitotic cells (Howard & Hyman, 2007). To test potential antagonism between Msps and Klp10A during dendrite pruning, we further eliminated Klp10A activity in *msps* RNAi ddaC

neurons to examine whether *msps* mutant phenotypes could be rescued. Remarkably, knockdown of *klp10A* (RNAi #1) in *msps* RNAi neurons significantly restored Nod- $\beta$ -gal distribution in dendrites (*n* = 16, Fig 6B and M), compared to *msps*, control RNAi neurons (*n* = 16, Fig 6A and M). Consistently, knockdown of *klp10A* in *msps*<sup>810</sup>/*msps*<sup>P18</sup> neurons significantly restored the retrograde movement of dendritic EB1-GFP comets (*n* = 29 neurons, 143 comets, Fig 7B and G), compared to the *msps*<sup>810</sup>/*msps*<sup>P18</sup> controls (*n* = 20 neurons, 150 comets, Fig 7A and G). Moreover, knockdown of *klp10A* largely restored overall MT levels in dendrites of *msps* RNAi neurons (*n* = 19; Fig EV4A). These data suggest an antagonism between Msps and Klp10A in regulating MT orientation and density in dendrites. More strikingly, both dendrite pruning and dendrite arborization defects in *msps* RNAi ddaC neurons were almost fully rescued by knockdown of *klp10A* (*n* = 16; Fig 6H, O and P), in contrast to those in *msps*, control RNAi neurons (*n* = 12; Fig 6G, O and P). As a control, knockdown of *klp10A* alone did not disturb dendrite pruning in ddaC neurons (*n* = 31, Fig 6O and P). Thus, these data suggest that the antagonism between Msps and Klp10A is important for both dendritic MT orientation and dendrite pruning.

Given that both impaired MT orientation and reduced MT density were observed in dendrites of *msps* mutant ddaC neurons, we next investigated which one might lead to the dendrite pruning defect in *msps* neurons. To this end, we examined two other MT-related proteins (Prefoldin5/Pfdn5 and Futsch) that regulate tubulin assembly or MT stability (Geissler *et al.*, 1998; Hummel *et al.*, 2000). Although knockdown of *pfdn5* or *futsch* showed a significant reduction in the number of EB1-GFP comets (Fig EV4C), dendritic MT orientation was not impaired (Fig EV4C). Overall MT density was significantly reduced in the dendrites of *pfdn5* RNAi ddaC dendrites (*n* = 15; Fig EV4B). Importantly, dendrite pruning was not affected in either *pfdn5* or *futsch* RNAi ddaC neurons (*n* = 19 and 15, respectively; Fig EV4D). Thus, these data suggest that impaired MT orientation, rather than reduced MT density, is likely responsible for the dendrite pruning defects.

### Excessive MT depolymerization perturbs dendritic MT orientation and dendrite pruning

Msps functions are antagonized by the MT depolymerase Klp10A, raising the possibility that excessive MT depolymerization might lead to dendritic MT orientation and dendrite pruning defects in

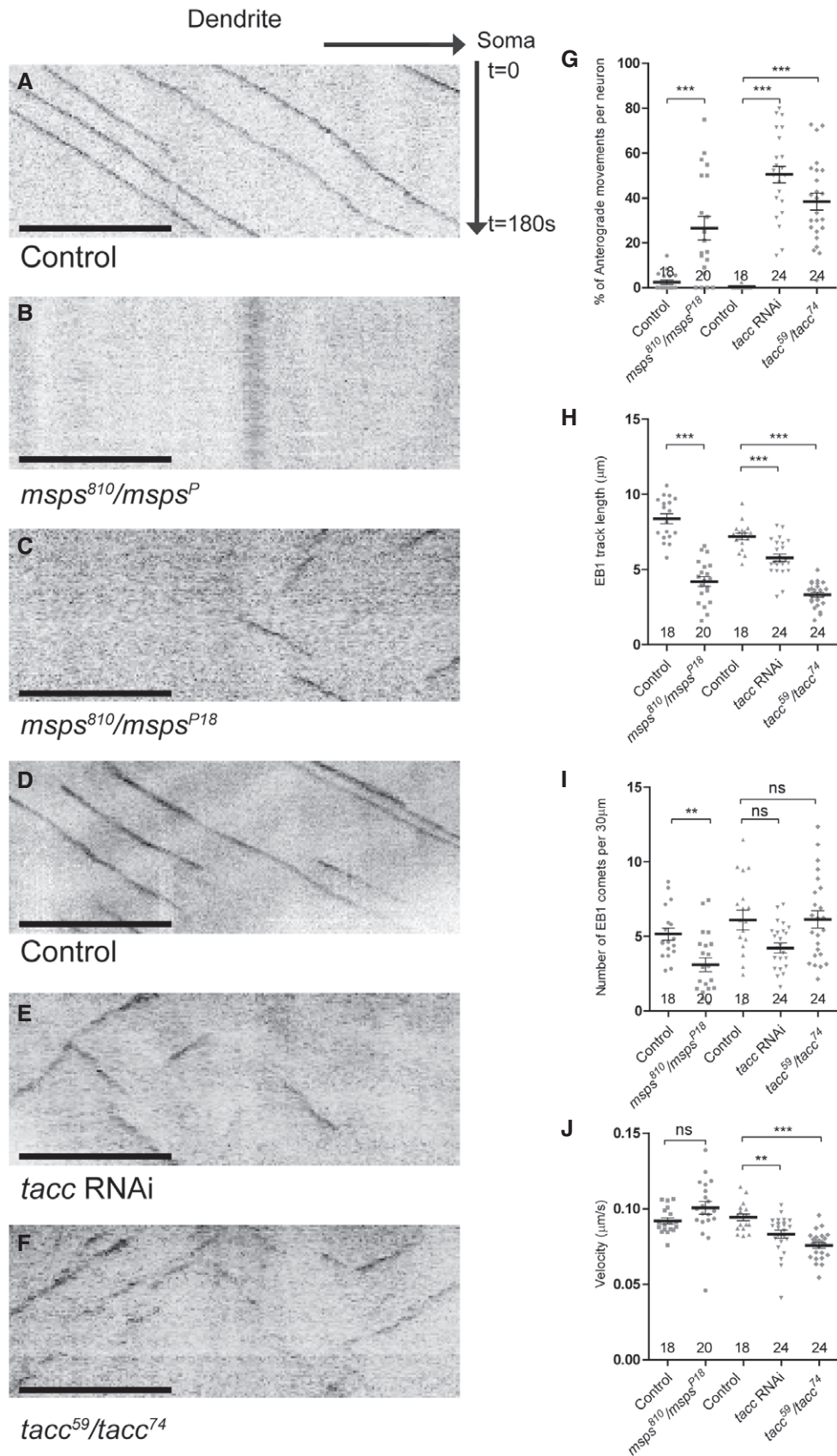


Figure 5.

**Figure 5. *mmps* and *tacc* are required for minus-end-out MT orientation in dendrites.**

A–F Representative kymographs depicting EB1 comet movement patterns in the proximal dendrites of *ddaC* neurons at 96 h AEL. Horizontal arrow indicates the direction toward the somas, and vertical arrow indicates the time. EB1::GFP expression was driven under *Gal4<sup>4-77</sup>*. In the control *ddaC* neurons (A, D), EB1 comets move predominantly in retrograde direction. EB1 comets were largely diminished in *mmps<sup>810</sup>/mmps<sup>P</sup>* mutant neurons (B). Interestingly, in *mmps<sup>810</sup>/mmps<sup>P18</sup>* mutants (C), *tacc* RNAi (E), and *tacc<sup>59</sup>/tacc<sup>74</sup>* mutant (F), increased anterograde comets were detected in *ddaC* dendrites.

G–J Quantitative analysis of the percentages of anterograde EB1::GFP comets, the track length, the number (per 30  $\mu$ m), and the velocity of the comets in each neuron imaged.

Data information: In (G–J), the numbers above the x-axis represent the sample sizes. Error bars represent SEM from three independent experiments. Statistical significances were determined by two-tailed Student's *t*-test (pairwise comparisons) or one-way ANOVA with Bonferroni test (multiple-group comparisons), \*\**P* < 0.01, \*\*\**P* < 0.001, ns indicates statistically not significant. Scale bar in (A–F) represents 10  $\mu$ m. Each kymograph was generated by analyzing a 3-min movie.

Source data are available online for this figure.

*mmps* mutant neurons. To examine this possibility, we induced MT depolymerization via both pharmacological and genetic approaches. First, we took advantage of two well-characterized MT-destabilizing agents (MDAs), namely colchicine and vinblastine. Colchicine and vinblastine were reported to induce MT catastrophe at the plus ends (Mohan *et al*, 2013). We first optimized a low concentration of colchicine and fed 72 h AEL larvae for 1 or 2 days. Under such a mild treatment condition, animals completed head eversion at 12 h APF and survived until the pharate adult stage, suggesting normal progression of metamorphosis. Moreover, this mild colchicine treatment did not affect the average number of primary and secondary dendrites in *ddaC* neurons at WP stage ( $n = 14$ ; Fig 6J and Appendix Fig S6A). Strikingly, Nod- $\beta$ -gal exhibited drastic accumulation in the soma with a severe reduction in the dendrites (22% of the control intensity) in all neurons ( $n = 16$ ; Fig 6D and N), compared to non-treated controls ( $n = 12$ ; Fig 6C and N). In the larvae treated with colchicine at a lower concentration, anterograde EB1-GFP comets were significantly increased to 15% in the dendrites ( $n = 31$  neurons, 402 comets; Fig 7D and G), compared to approximately 2% in the control neurons ( $n = 24$  neurons, 313 comets; Fig 7C and G), indicative of a MT orientation defect. The average track length of EB1-GFP comets was reduced in those *ddaC* neurons from the colchicine-treated larvae (Fig 7H). Concomitantly, dendrite severing defects were also observed in the majority of *ddaC* neurons from colchicine-treated animals at 16 h APF (74%,  $n = 31$ ; Fig 6J, O and P), compared to no defect in the non-treated neurons (0%,  $n = 29$ ; Fig 6I, O and P). Likewise, when vinblastine was fed, *ddaC* neurons also exhibited a significant reduction in Nod- $\beta$ -gal signals ( $n = 31$ ; Appendix Fig S6B) and an increase in anterograde EB1-GFP comets ( $n = 9$  neurons; Appendix Fig S6C) in dendrites. The mild vinblastine treatment did not compromise the average number of primary and secondary dendrites in *ddaC* neurons at WP stage ( $n = 10$ , Appendix Fig S6A), however led to consistent dendrite pruning defects in most of the neurons at 16 h APF (69%,  $n = 15$ ; Appendix Fig S6D). Thus, these data indicate that the treatment of colchicine and vinblastine, two MT depolymerization drugs, impairs dendritic MT orientation and dendrite pruning.

Next, we genetically depolymerized MTs by overexpressing katanin, a MT-severing AAA+ ATPase. Katanin is a heterodimer consisting two subunits, p60 (Kat-60) that possesses the microtubule-severing enzymatic activity and p80 (Kat-80) that regulates the activity and targeting of p60 (Yu *et al*, 2005). *Drosophila* Kat-60 has been shown to disassemble tubulin dimers from MT ends to depolymerize MT filaments (Diaz-Valencia *et al*, 2011; Mao *et al*,

2014). Two previous reports showed that knockdown of *kat-60* via various RNAi lines did not affect dendrite pruning in *ddaC* neurons (Lee *et al*, 2009; Tao *et al*, 2016), whereas loss of its paralog *kat-60L1* led to dendrite pruning defects (Lee *et al*, 2009). We found that Kat-60 but not Kat-60L1 formed a complex with Kat-80 in the co-IP experiments (Fig EV5A), suggesting that Kat-60, rather than Kat-60L1, functions as a catalytic subunit of katanin. Interestingly, when we overexpressed Kat-60 in *ddaC* neurons via *ppk-Gal4* driver, Nod- $\beta$ -gal signals accumulated in soma with a significant reduction in dendrites (25% of the control intensity) in all neurons ( $n = 23$ ; Fig 6F and N), compared to normal Nod- $\beta$ -gal distribution in the control neurons ( $n = 15$ ; Fig 6E and N). In Kat-60-overexpressing *ddaC* neurons, anterograde EB1-GFP comets were drastically increased to 40% in the dendrites ( $n = 22$  neurons, 622 comets; Fig 7F and G), compared to approximately 2% in the control neurons ( $n = 13$  neurons, 132 comets; Fig 7E and G). The average track length of EB1-GFP comets drastically decreased (Fig 7H), whereas the average EB1-GFP comet number significantly increased in these neurons (Fig 7I). However, the average velocity of EB1-GFP comets remained unaltered (Fig 7J). Importantly, Kat-60 overexpression resulted in ectopic branches at the proximal dendrites of all *ddaC* neurons ( $n = 18$ , Fig 6L), which were also observed in *mmps* or *tacc* mutant neurons (Appendix Fig S1A and Fig EV2C). Dendrite severing was inhibited in most of Kat-60-overexpressing *ddaC* neurons at 16 h APF (63%,  $n = 30$ ; Fig 6L, O and P), compared to no severing defect in the control neurons (0%,  $n = 29$ ; Fig 6K, O and P). In contrast, Kat-60L1 overexpression did not affect dendrite pruning ( $n = 15$ ; Fig EV5B). Finally, similar to that in *mmps* RNAi neurons, overall microtubule levels were significantly reduced in dendrites of colchicine/vinblastine-treated and Kat-60-overexpressing *ddaC* neurons (Fig EV5C), as detected by the anti- $\alpha$ -Tubulin antibody. Thus, MDA treatment and katanin overexpression phenotype *mmps* mutants.

In summary, we provide multiple lines of genetic, cell biological, and pharmacological evidence demonstrating that the conserved MT polymerase *Mmps* is required to form minus-end-out MTs in dendrites and thereby promotes dendrite pruning in *ddaC* sensory neurons (Fig 8).

## Discussion

Despite that MT disassembly precedes neuronal pruning, major MT-severing factors appear to be dispensable for dendrite pruning in

ddaC neurons (Lee et al, 2009; Stone et al, 2014; Tao et al, 2016). Here, we have identified an unexpected role of a key MT polymerase Msp in dendrite pruning of ddaC neurons. First, genetic analyses with *msps* mutants, the rescue experiments, and additional

RNAi lines highlight an important role of *msps* in regulating dendrite pruning in ddaC neurons. Second, we show that Msp forms an *in vivo* protein complex with TACC in adult neurons; both proteins stabilize each other in ddaC neurons independently of MT

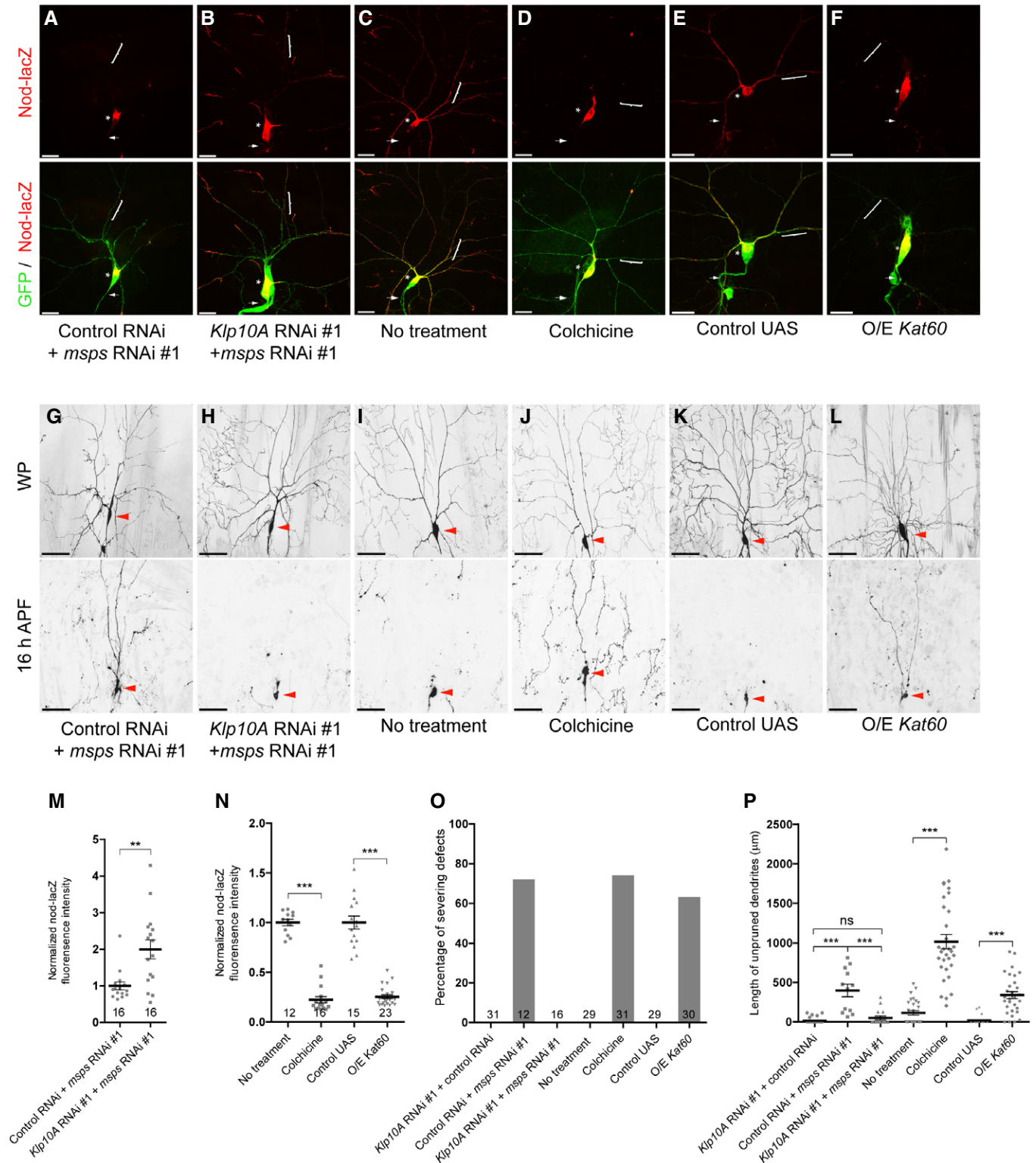


Figure 6.

**Figure 6. Excessive MT depolymerization perturbs dendrite pruning.**

- A–F Confocal images of ddaC neurons expressing *UAS-mCD8::GFP* (Green channel) and *UAS-Nod-lacZ* and immunostained for  $\beta$ -galactosidase at wL3 stages. Simultaneous knockdown of *klp10A* and *mmps* (B) significantly restored Nod-lacZ localization in the dendrites, compared to *mmps* and control RNAi (A). ddaC neurons with colchicine treatment (D) or with Kat-60 overexpression (F) exhibited perturbed Nod-lacZ distribution with highly enriched staining in the soma and decreased signals in the dendrites. Asterisks indicate the location of ddaC somas. White arrows indicate the location of axons. Curly brackets mark the dendritic regions where fluorescence intensity of Nod-lacZ was measured.
- G–L Live confocal images of ddaC neurons visualized by *ppk-Gal4*-driven *mCD8::GFP* expression at WP or 16 h APF. Simultaneous knockdown *klp10A* and *mmps* (H) almost fully rescued the dendrite morphological defects and the pruning defects compared with the *mmps*, control RNAi neurons. Wild-type larvae fed with colchicine (J) showed pruning defects in comparison with those fed with DMSO (I). ddaC neurons with *Kat-60* overexpression (L) exhibited abnormal dendrite arborization and pruning defects. Red arrowheads point to the ddaC somas.
- M, N Quantitative analysis of normalized Nod-lacZ intensity for 20  $\mu$ m of major dendrite located 55  $\mu$ m or 40  $\mu$ m away from the soma, respectively.
- O Percentages of ddaC neurons showing severing defects at 16 h APF.
- P Quantitative analysis of unpruned dendrite lengths at 16 h APF.

Data information: In (M–O), the numbers above the x-axis represent the sample sizes. Error bars represent SEM from three independent experiments. In (M, N, P), statistical significance was determined by two-tailed Student's t-test (pairwise comparisons in M, N, P) or one-way ANOVA with Bonferroni test (multiple-group comparison in P), \*\* $P < 0.01$ , \*\*\* $P < 0.001$ . Scale bars in (A–F) and (G–L) represent 20  $\mu$ m and 50  $\mu$ m, respectively.

Source data are available online for this figure.

mass. Third, TACC, like Msps, is required for dendrite pruning. Fourth, the dendrite pruning defects in *mmps* knockdown neurons are likely caused by excessive Klp10A, a MT-depolymerizing kinesin. Consistently, excessive MT depolymerization, which is induced by both MDA treatment and katanin overexpression, resembles all *mmps* loss-of-function phenotypes with regard to both dendritic MT orientation and pruning. Thus, Msps plays an important role in dendrite pruning in ddaC sensory neurons (Fig 8).

The vertebrate orthologs of Msps were reported to regulate MT dynamics and axon outgrowth in neurons from frogs and mammals (van der Vaart *et al*, 2012; Lowery *et al*, 2013), but their roles in neuronal MT orientation remain unknown in both invertebrates and vertebrates. In this study, we demonstrate, for the first time, that Msps and its binding partner TACC play an important role in governing minus-end-out orientation of dendritic MTs, which is very likely required for dendrite pruning in ddaC sensory neurons. TACC is able to recruit Msps to centrosomal MTs during mitosis, and both proteins move toward the plus ends in mitotic cells of early *Drosophila* embryos (Lee *et al*, 2001). Thus, TACC might also target Msps to the MT plus ends to polymerize minus-end-out MTs in the dendrites of ddaC neurons.

How does Msps regulate MT minus-end-out orientation in ddaC dendrites? Msps might associate with the MT plus ends and promote persistent MT growth against MT depolymerization events in ddaC dendrites, which leads to the formation of long and stable MT filaments. Plus-end motors kinesins, via MT guidance or sliding, may orient growing MTs in a minus-end-out orientation in the dendrites (Mattie *et al*, 2010; Yan *et al*, 2013). These minus-end-out MTs may form stable bundles that anchor within the dendrites. In the absence of Msps, dendritic MTs are depolymerized from their plus ends or along the lattices mediated by excessive depolymerization activity of kinesin-13 and/or other MT-severing factors. It has been shown that microtubule-severing factors are able to sever MTs into short pieces (McNally & Vale, 1993), which may serve as MT seeds. Short MT seeds might be re-oriented in either plus-end-out or minus-end-out direction with equal probability, resulting in a mixed MT polarity in the dendrites of *mmps* mutant neurons. In line with this idea, knockdown of the MT-depolymerizing factor Klp10A in *mmps* mutant neurons significantly restored minus-end-out MT filaments in the dendrites. Moreover, MDA treatments and Kat-60

overexpression that depolymerize MTs from the MT ends also led to mixed MT orientation in dendrites, identical to *mmps* loss-of-function mutants. The Msps vertebrate ortholog XMAP215 interacts with  $\gamma$ -tubulin via its carboxyl-terminal portion to synergistically stimulate MT nucleation *in vitro* (Thawani *et al*, 2018). Interestingly,  $\gamma$ -tubulin was reported to regulate the minus-end-out MT orientation in dendrites of class I da sensory neurons (Nguyen *et al*, 2014). It is conceivable that Msps and  $\gamma$ -tubulin might be part of the asymmetric MT nucleation machinery which is responsible for the generation of non-centrosomal MTs with a minus-end-out orientation in dendrites of ddaC neurons. Unexpectedly, we found no notable biochemical/genetic interaction between Msps and  $\gamma$ -tubulin in *Drosophila*. Future studies will be required to identify such an asymmetric MT nucleation/polymerization machinery in neurons.

Our study supports a link between dendritic MT orientation and dendrite pruning defect. Both *mmps* and *TACC* mutant ddaC neurons, which showed impaired MT orientation in dendrites, had dendrite pruning defects. Moreover, knockdown of *klp10A* restored the minus-end-out MT orientation in dendrites and rescued the dendrite pruning defect in *mmps* RNAi or mutant neurons. MDA treatment and katanin overexpression led to impaired MT orientation as well as dendrite pruning defects, phenocopying *mmps* mutant neurons. Growing evidence supports a likely causal link between minus-end-out MT orientation and dendrite pruning. First, Cnn and APC1/2, two known regulators of dendritic MT orientation (Mattie *et al*, 2010; Yalgin *et al*, 2015), are required for dendrite pruning (Wang *et al*, 2019). Second, the Rumpf laboratory has recently reported that both *kinesin-1* and *kinesin-2* mutant ddaC neurons that exhibited mixed dendritic MT orientations (Mattie *et al*, 2010) had dendrite pruning defects (Herzmann *et al*, 2018). Third, we and others have recently reported that the MT minus-end-binding protein Patronin, which also regulates uniform minus-end-out MT orientation in dendrites (Feng *et al*, 2019; Wang *et al*, 2019), is also critical for dendrite pruning (Wang *et al*, 2019). In contrast, we further show here that knockdown of other MT-related proteins, Pfdn5 and Futsch, which did not affect minus-end-out MT orientation in dendrites, did not cause any dendrite pruning defect in ddaC neurons. Thus, all these data strongly support a likely causal link between minus-end-out MT orientation and dendrite pruning.

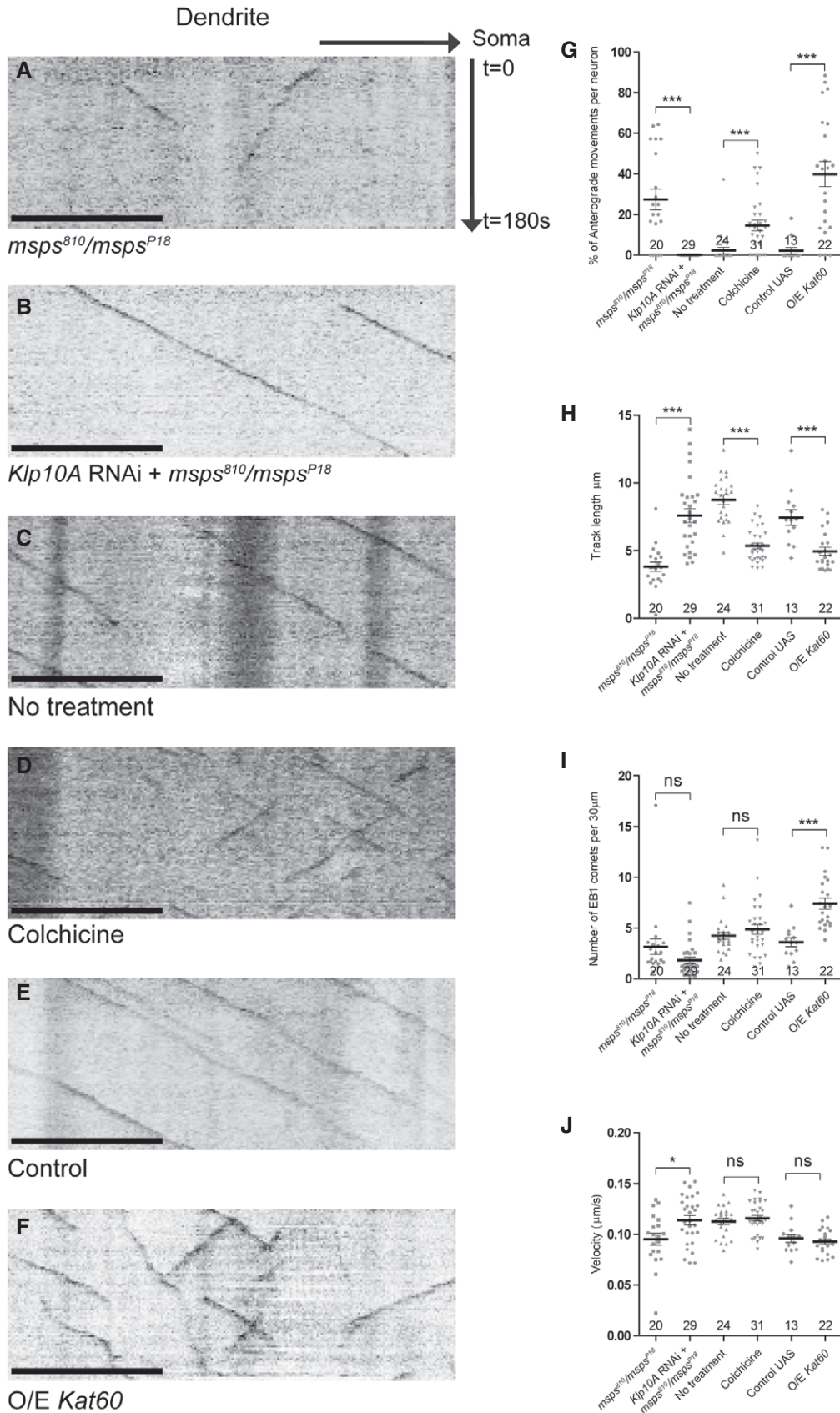


Figure 7.

**Figure 7. Excessive MT depolymerization perturbs dendritic MT orientation.**

A–F Representative kymographs depicting EB1 comet movement patterns in the proximal dendrites of *ddaC* neurons at 96 h AEL. Horizontal arrow indicates the direction toward the somas, and vertical arrow indicates the time. (B) RNAi knockdown of *klp10A* in *mssp<sup>210</sup>/mssp<sup>218</sup>* mutants restored the retrograde movement pattern of EB1 comets. MT depolymerization or severing induced by colchicine treatment (D) or overexpression of *Kat-60* (F) led to mixed MT orientation in *ddaC* neurons.

G–J Quantitative analysis of the percentages of anterograde EB1 comets, the track length, number (per 30  $\mu$ m), and the velocity of EB1 comets in each neuron imaged. Data information: In (G–J), the numbers above the x-axis represent the sample sizes. Error bars represent SEM from three independent experiments. Statistical significances were determined by two-tailed Student's *t*-test, \**P* < 0.05, \*\*\**P* < 0.001, ns indicates statistically not significant. Scale bar in (A–F) represents 10  $\mu$ m. Source data are available online for this figure.

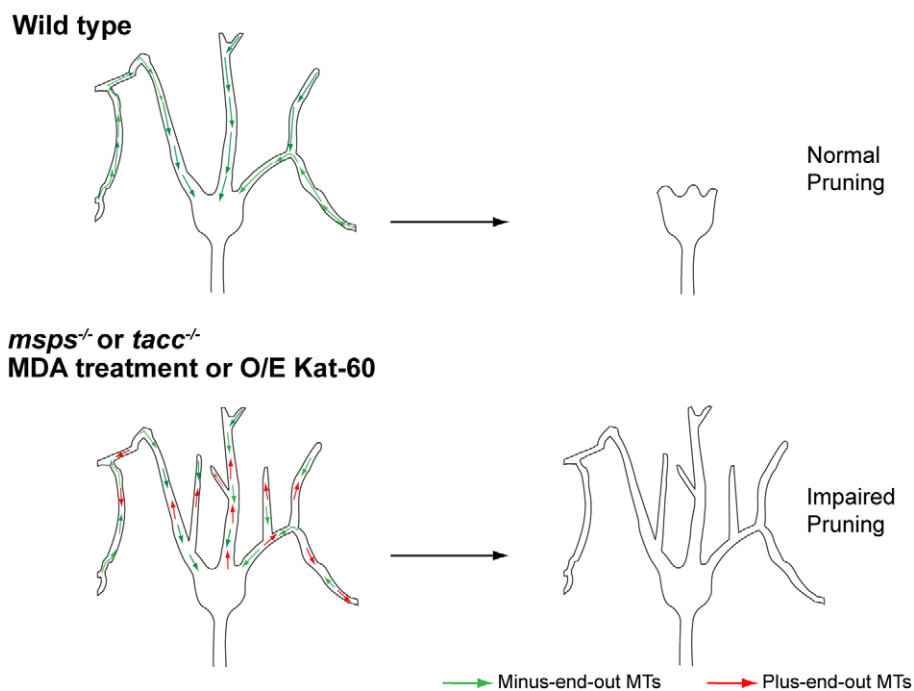
How mis-oriented MT arrays impact on dendrite pruning is currently unknown. It is conceivable that dendrites with a minus-end-out MT orientation might be more susceptible to dendrite pruning. Severing of dendrites usually takes place at proximal region of dendrite arbors, where the plus ends of MTs are enriched, raising the possibility that the dynamic plus ends are more prone to severing and disassembly. Alternatively, organelles, for example, endosomes and lysosomes, move along the minus-end-out dendritic MTs in *ddaC* neurons (Satoh *et al*, 2008), which might facilitate the efficient endo-lysosomal degradation of Nrg during dendrite pruning (Zhang *et al*, 2014).

In summary, this study reveals a new paradigm that a conserved MT polymerase *Msp*s plays an important role in dendrite pruning in *Drosophila* sensory neurons. Furthermore, we show that *Msp*s is required to regulate dendritic MT orientation and thereby promotes dendrite pruning.

**Materials and Methods****Fly strains**

*ppk-Gal4* on II and III chromosome (Grueber *et al*, 2003), *SOP-flp* (#42) (Matsubara *et al*, 2011), *mssp<sup>D</sup>* (Cullen *et al*, 1999), *g-mssp* (HN267) (Cullen *et al*, 1999), *UAS-Mical<sup>N-ter</sup>* (Terman *et al*, 2002), *UAS-EB1-GFP* (Stone *et al*, 2008), *UAS-Kin- $\beta$ -gal* (Clark *et al*, 1997), *UAS-Venus-Kat-60L1* (Stewart *et al*, 2012), *UAS-ManII-Venus* (Wang *et al*, 2017), *UAS-ManII-GFP* (Ye *et al*, 2007), *UAS- $\gamma$ Tub23C-GFP* (Nguyen *et al*, 2014), *mssp<sup>P18</sup>* (Chen *et al*, 2016), *puc-lacZ* (Martin-Blanco *et al*, 1998), *tacc<sup>59</sup>*, *tacc<sup>74</sup>*, *mssp<sup>810</sup>*, and *mssp<sup>924</sup>* (this study).

The following stocks were obtained from Bloomington Stock Centre (BSC): *UAS-mCD8::GFP*, *FRT82B*, *UAS-Dicer2*, *tacc* RNAi #1 (BL#65982), *ppk-CD4-tdGFP* (BL#35842), *Gal4<sup>4-77</sup>* (BL#8737), *UAS-*

**Figure 8. A working model.**

In wild-type, *ddaC* neurons establish minus-end-out MT orientation which is likely required for dendrite pruning. In *mssp* or *tacc* mutant neurons, minus-end-out MT orientation in dendrites is disrupted, which likely results in impaired dendrite pruning. MT depolymerization, which is induced by both MDA treatment and katanin overexpression, also causes mixed MT orientation in dendrites as well as dendrite pruning defects. This study supports a link between minus-end-out MT orientation and dendrite pruning.



*CD4-tdTom* (BL#35841), *UAS-Nod-β-gal* (BL#9912), *nanos-Cas9* (BL#54591), *k1p10A* RNAi # 1 (BL#33963), *tubP-Gal80*, *Gal4<sup>109(2)80</sup>*, *elav-Gal4<sup>C155</sup>* (BL#458), *UAS-Kat-60* (BL#64115), *UAS-Mito-GFP* (BL#8442), *γ-tub23C<sup>A15-2</sup>* (BL#7042), *γ-tub23C<sup>A14-9</sup>* (BL#7041), *UAS-JNK<sup>DN</sup>(Bsk<sup>DN</sup>)* #1 (BL#6409), and *UAS-JNK<sup>DN</sup>(Bsk<sup>DN</sup>)* #2 (BL#9311).

The following stocks were obtained from the Vienna *Drosophila* RNAi Centre (VDRC): *msps* RNAi #1 (v21982), control RNAi (v36355, v25271), *tacc* RNAi #2 (v101439), *γ-tub23C* RNAi (v19130), *futsch* RNAi (v6972), *pdfn5* RNAi (v29812), and *α-tub84B* RNAi (v33427).

The following stocks were obtained from National Institute of Genetics, Japan: *msps* RNAi #2 (5000R-3).

### EMS mutagenesis

Isogenized *w<sup>\*</sup>;FRT82B* male flies were fed with 25 mM EMS. Mutant chromosomes were balanced over TM6B prior to isolation of lethal or semi-lethal lines. These lines were then used for the following MARCM analysis.

### MARCM analysis of da neurons

Embryos were collected every 1–2 days and cultivated on cornmeal food at 25°C. For analyzing dendrite phenotype of *ddaC*, *ddaD/E*, or *ddaF* neurons, animals at WP stage were first collected onto moisturized tissue paper at 25°C overnight. Pupal cases were removed for confocal imaging of da neurons at 16 or 19 h APF correspondingly. MARCM clones labeled by GFP were analyzed using confocal Microscopy.

### Brain protein extraction for Western blot and co-immunoprecipitation (co-IP)

Larval brains or adult fly heads were dissected and ground in 1 to 1 mixture of lysis buffer (Pierce, Cat#87788) and loading dye. Standard Western blots were conducted immediately to analyze protein contents. For co-IP, flies were collected and decapitated by vigorous shaking after frozen. The lysis buffer (Pierce, Cat#87788) with freshly added protease inhibitor (Roche, Cat#11697498001) was used to extract proteins from the fly heads. GFP or Venus-tagged proteins were immunoprecipitated with anti-GFP beads (Chromotek, GFP-Trap A) and subjected to standard Western blot analyses. Each Western blot or co-IP assay was repeated for 3–6 times.

### Cell culture and co-IP

S2 cells were maintained in Express Five SFM (Life Tech) supplemented with 1% L-glutamine (Life Tech) at 25°C. Transfections of destination vectors were conducted following Qiagen Effectene transfection procedure (Qiagen, Cat#301427). Transfected S2 cells were homogenized with lysis buffer (25 mM Tris pH 8, 27.5 mM NaCl, 20 mM KCl, 25 mM sucrose, 1 mM DTT, 10% (v/v) glycerol, 0.5% NP40, and protease inhibitors), as previously described (Wong et al, 2013). Standard Western blot was then conducted to analyze co-immunoprecipitated protein components. Each co-IP assay was repeated for three times.

### Immunohistochemistry

wL3 larvae and WP samples for each set of experiments were dissected in cold PBS and processed simultaneously. For Futsch (22C10) and  $\alpha$ -tubulin staining, the following fixation procedures were performed in order to assess MT mass without unpolymerized tubulin subunits. Larvae were dissected in cold Ca<sup>2+</sup>-free HL3.1 saline, and their muscles were removed (Yalgin et al, 2011; Tenenbaum & Gavis, 2016). The dissected fillets were fixed in freshly prepared PHEM fixing buffer with 0.25% glutaraldehyde, 3.7% paraformaldehyde, 3.7% sucrose, and 0.1% Triton X-100. The samples were then quenched with 50 mM ammonium chloride for 5 min (Witte et al, 2008). The samples within the same group of experiments were stained in the same tube and mounted in VECTA-SHIELD mounting medium. The samples were directly visualized by Leica SPE-II confocal microscope and processed in parallel. Data analysis and statistics were performed via Excel (Microsoft) and GraphPad Prism software.

### Antibodies

The following antibodies and dilutions were used in this study: Guinea pig anti-Msps (IF 1:500, WB 1:3,000, a gift from H. Wang), rabbit anti-TACC (IF 1:500; WB 1:3,000, a gift from J.W. Raff and H. Wang), mouse anti-β-Galactosidase (IF 1:1,000, Promega, Cat#Z3781), rabbit anti-GFP (WB 1:5,000, Invitrogen, Cat#A-11122), mouse anti-Futsch (IF 1:50, 22C10, DSHB), rabbit anti-beta actin (WB 1:3000, Abcam, Cat#ab8227), mouse anti-alpha tubulin (WB 1:3,000, IF 1:500, Sigma, Cat#T9026), mouse anti-γ-tubulin (1:500, Sigma, Cat#T5326), Rabbit anti-Patronin (a gift from M. Gonzalez-Gaitan, 1:500), mouse anti-Myc (WB 1:3,000, Sigma, Cat#M4439), mouse anti-Myc-HRP (WB 1:10,000, Invitrogen, Cat#R951-25), rabbit anti-Flag (WB 1:3,000, Sigma, Cat#F7425), mouse anti-Flag-HRP (WB 1:10,000, Sigma, Cat#A8592), Cy3-conjugated goat anti-mouse antibody, Cy3-conjugated goat anti-Guinea pig antibody, 488-conjugated goat anti-rabbit antibody, Cy3-conjugated goat anti-rabbit antibody, and 649-conjugated goat anti-HRP antibody (IF 1:500, Jackson Laboratories, Cat#115-165-003, Cat#106-165-003, Cat#111-545-003, Cat#111-165-003, Cat#123-495-021).

### MDA treatments

Embryos were collected at 12-h intervals and cultivated on standard food. The larvae were then transferred to the food containing 20 μg/ml colchicine (Sigma Aldrich Cat#C9754), 15 μM vinblastine (Tocris Cat#1256), or 50 μM GNE-3511 (Millipore CAS#5.33168.0001). WPs were collected after 1–2 days of drug feeding and used for confocal imaging at 16 h APF. Wandering 3<sup>rd</sup> instar larvae were collected after 1–2 days of drug feeding and used for anti-β-gal staining. For EB1-GFP movies, a lower concentration of 1 μg/ml colchicine, 12 μM vinblastine, or 50 μM GNE-3511 was used for the treatment, and 96 h AEL larvae were collected after 1 day of drug feeding and used for live imaging of EB1-GFP.

### Plasmid construction

The coding sequences of *msps*, *tacc*, *kat-60*, *kat-60L1*, and *kat-80* were amplified from EST clones (DGRC, Bloomington). The

respective fragments were cloned into Gateway entry vectors pENTR/D-TOPO or pDONR/Zeo (Invitrogen), followed by cloning into Gateway destination vectors (pAMW, pAFW) (DGRC) via LR reaction.

### Generation of *tacc* mutants via CRISPR/Cas9

Two different guide RNAs (gRNAs) targeting *tacc* exons were cloned into the pCFD4 vector following the standard procedures published previously (Port *et al*, 2014). The following primer set was used: 5'-TATATAGGAAAGATATCCGGGTGAACCTTCGCAACGTCAGCTATGAAGCCAGTTTTAGAGCTAGAAATAGCAAG-3', 5'-ATTTTAACTTGCTATTTCTAGCTCTAAAACCTCTCACTAATGAGCTCTGCACGACGTTAAATTGAAAAATAGGTC-3'. Transgenic flies were generated by BestGene Inc and crossed with *nanos-Cas9* flies to generate mutant *tacc* lines. Mutants with large genomic deletions were isolated by PCR and confirmed by DNA sequencing. Embryo microinjection services were provided by BestGene Inc.

### Live imaging of EB1-GFP comet

Larvae at desired developmental stages were immersed with halocarbon oil (Santa Cruz, Cat#sc-250077) and mounted to slides for confocal imaging. Time-lapse imaging of EB1-GFP comet was performed with Olympus FV3000 using 60 $\times$  oil lens with 3 $\times$  zoom. Eighty-three frames were acquired at 2.25-s intervals with 6 Z-steps. Kymographs were generated for Z-projected time-lapse images using KymographBuilder plugin in ImageJ.

### Analysis of ddaC dendrites

Dendrite images for larvae and WP were taken using Leica SPE-II with 40 $\times$  oil lens. To image full arbor of ddaC neurons at different stages, multiple images were acquired and stitched using ImageJ plugin MosaicJ. Dendritic termini number was calculated using ImageJ plugin Simple Neurite Tracer. The severing defect was defined by the presence of dendrites that remain attached to the soma at 16 h APF. The total length of unpruned dendrites was measured in a 275  $\times$  275  $\mu$ m region of the dorsal dendritic field using ImageJ. Sholl analyses of dendrite morphogenesis were conducted using ImageJ. Plots of average length, number of intersections, and SEM were generated using GraphPad Prism software.

### Quantification of immunostaining

Images were acquired from projected z-stacks (at 1.5  $\mu$ m intervals) to cover the entire volume of ddaC/D/E sensory neurons using the confocal microscopy Leica TSC SP2. To quantify the fluorescence intensities, cell nuclei (*pu*-lacZ) or whole soma (Patronin/Msps/TACC immunostaining) contours were drawn on the appropriate fluorescent channel based on the GFP channel or relative cellular position in ImageJ software. After subtracting the background (Rolling Ball Radius = 30) on the entire image of that channel, we measured the mean gray value in the marked area in ddaC and/or ddaE on the same images and calculated their ratios. The ratios were normalized to the corresponding average control values and subjected to statistical analysis for comparison between different

conditions. Graphs display the average values of ddaC soma/nucleus or ddaC/ddaE ratios and the standard error of the mean (SEM) normalized to controls. The number of ddaC neurons (n) examined in each group is shown on the bars. Insets show the ddaC neurons labeled by *ppk-Gal4*-driven *UAS-mCD8-GFP* expression.

To quantify the alterations of dendritic Nod- $\beta$ -gal distribution, we measured its intensity in the 20  $\mu$ m of major dorsal dendrites which were 40  $\mu$ m away from the soma. The number of ddaC neurons (n) examined in each group is shown on the bars. Dorsal is up in all images.

### Statistics

For pairwise comparison, two-tailed Student's *t*-test was applied to determine statistical significance. One-way ANOVA with Bonferroni test was applied to determine significance when multiple groups were present. Error bars in all graphs represent standard error of the mean (SEM). Statistical significance was defined as \*\*\**P* < 0.001, \*\**P* < 0.01, \**P* < 0.05, n.s., not significant. The number of samples (n) in each group is shown on the bars.

**Expanded View** for this article is available online.

### Acknowledgements

We thank Y. Jan, H.T. Broihier, C.A. Collins, P. Léopold, H. Ohkura, A. Prokop, J.W. Raff, S. Rogers, M.M. Rolls, T. Uemura, H. Wang, the Bloomington Stock Center (BSC), DSHB (University of Iowa), Kyoto Stock Center (Japan), and VDRC (Austria) for generously providing antibodies and fly stocks. We thank A. Moore and Yu lab members for helpful discussion and B. Lim for technical assistance. This work was supported by Temasek Life Sciences Laboratory Singapore (TLL-2040) and National Research Foundation Singapore (SBP-P3 and SBP-P8) (F.Y.).

### Author contributions

FY, QT, and YW conceived and designed the study. QT performed most of the experiments. MR conducted some Western blot and JNK experiments. SB performed some EB1-GFP movies, JNK, and drug treatment experiments. YW conducted some EB1-GFP and Nod- $\beta$ -gal experiments. LYC carried out some JNK experiments. QT, YW, and FY analyzed the data. FY and QT wrote the paper.

### Conflict of interest

The authors declare that they have no conflict of interest.

## References

- Akhmanova A, Steinmetz MO (2008) Tracking the ends: a dynamic protein network controls the fate of microtubule tips. *Nat Rev Mol Cell Biol* 9: 309–322
- Akhmanova A, Steinmetz MO (2015) Control of microtubule organization and dynamics: two ends in the limelight. *Nat Rev Mol Cell Biol* 16: 711–726
- Al-Bassam J, Chang F (2011) Regulation of microtubule dynamics by TOG-domain proteins XMAP215/Dis1 and CLASP. *Trends Cell Biol* 21: 604–614
- Baas PW, Deitch JS, Black MM, Banker GA (1988) Polarity orientation of microtubules in hippocampal neurons: uniformity in the axon and nonuniformity in the dendrite. *Proc Natl Acad Sci USA* 85: 8335–8339
- Bellanger JM, Gonczy P (2003) TAC-1 and ZYG-9 form a complex that promotes microtubule assembly in *C. elegans* embryos. *Curr Biol* 13: 1488–1498

- Brouhard GJ, Stear JH, Noetzel TL, Al-Bassam J, Kinoshita K, Harrison SC, Howard J, Hyman AA (2008) XMAP215 is a processive microtubule polymerase. *Cell* 132: 79–88
- del Castillo U, Winding M, Lu W, Gelfand VI (2015) Interplay between kinesin-1 and cortical dynein during axonal outgrowth and microtubule organization in *Drosophila* neurons. *Elife* 4: e10140
- Chen K, Koe CT, Xing ZB, Tian X, Rossi F, Wang C, Tang Q, Zong W, Hong WJ, Taneja R et al (2016) Arl2- and Msps-dependent microtubule growth governs asymmetric division. *J Cell Biol* 212: 661–676
- Clark IE, Jan LY, Jan YN (1997) Reciprocal localization of Nod and kinesin fusion proteins indicates microtubule polarity in the *Drosophila* oocyte, epithelium, neuron and muscle. *Development* 124: 461–470
- Cullen CF, Deak P, Glover DM, Ohkura H (1999) mini spindles: a gene encoding a conserved microtubule-associated protein required for the integrity of the mitotic spindle in *Drosophila*. *J Cell Biol* 146: 1005–1018
- Cullen CF, Ohkura H (2001) Msps protein is localized to acentrosomal poles to ensure bipolarity of *Drosophila* meiotic spindles. *Nat Cell Biol* 3: 637–642
- Diaz-Valencia JD, Morelli MM, Bailey M, Zhang D, Sharp DJ, Ross JL (2011) *Drosophila* katanin-60 depolymerizes and severs at microtubule defects. *Biophys J* 100: 2440–2449
- Feng C, Thyagarajan P, Shorey M, Seebold DY, Weiner AT, Albertson RM, Rao KS, Sagasti A, Goetschius DJ, Rolls MM (2019) Patronin-mediated minus end growth is required for dendritic microtubule polarity. *J Cell Biol* 218: 2309–2328
- Geissler S, Siegers K, Schiebel E (1998) A novel protein complex promoting formation of functional alpha- and gamma-tubulin. *EMBO J* 17: 952–966
- Gergely F, Draviam VM, Raff JW (2003) The ch-TOG/XMAP215 protein is essential for spindle pole organization in human somatic cells. *Genes Dev* 17: 336–341
- Goodwin PR, Sasaki JM, Juo P (2012) Cyclin-dependent kinase 5 regulates the polarized trafficking of neuropeptide-containing dense-core vesicles in *Caenorhabditis elegans* motor neurons. *J Neurosci* 32: 8158–8172
- Grueber WB, Ye B, Moore AW, Jan LY, Jan YN (2003) Dendrites of distinct classes of *Drosophila* sensory neurons show different capacities for homotypic repulsion. *Curr Biol* 13: 618–626
- Gutierrez-Caballero C, Burgess SG, Bayliss R, Royle SJ (2015) TACC3-ch-TOG track the growing tips of microtubules independently of clathrin and Aurora-A phosphorylation. *Biol Open* 4: 170–179
- Han C, Song Y, Xiao H, Wang D, Franc NC, Jan LY, Jan YN (2014) Epidermal cells are the primary phagocytes in the fragmentation and clearance of degenerating dendrites in *Drosophila*. *Neuron* 81: 544–560
- Herzmann S, Krumkamp R, Rode S, Kintrup C, Rumpf S (2017) PAR-1 promotes microtubule breakdown during dendrite pruning in *Drosophila*. *EMBO J* 36: 1981–1991
- Herzmann S, Gotzelmann I, Reekers LF, Rumpf S (2018) Spatial regulation of microtubule disruption during dendrite pruning in *Drosophila*. *Development* 145: dev156950
- Honnappa S, Gouveia SM, Weisbrich A, Damberger FF, Bhavesh NS, Jawhari H, Grigoriev I, van Rijssel FJ, Buey RM, Lawera A et al (2009) An EB1-binding motif acts as a microtubule tip localization signal. *Cell* 138: 366–376
- Howard J, Hyman AA (2003) Dynamics and mechanics of the microtubule plus end. *Nature* 422: 753–758
- Howard J, Hyman AA (2007) Microtubule polymerases and depolymerases. *Curr Opin Cell Biol* 19: 31–35
- Hummel T, Krukkert K, Roos J, Davis G, Klambt C (2000) *Drosophila* Futsch/22C10 is a MAP1B-like protein required for dendritic and axonal development. *Neuron* 26: 357–370
- Hunter AW, Caplow M, Coy DL, Hancock WO, Diez S, Wordeman L, Howard J (2003) The kinesin-related protein MCAK is a microtubule depolymerase that forms an ATP-hydrolyzing complex at microtubule ends. *Mol Cell* 11: 445–457
- Kanamori T, Kanai MI, Dairyo Y, Yasunaga K, Morikawa RK, Emoto K (2013) Compartmentalized calcium transients trigger dendrite pruning in *Drosophila* sensory neurons. *Science* 340: 1475–1478
- Kanamori T, Togashi K, Koizumi H, Emoto K (2015) Dendritic remodeling: lessons from invertebrate model systems. *Int Rev Cell Mol Biol* 318: 1–25
- Kinoshita K, Noetzel TL, Pelletier L, Mechtler K, Drechsel DN, Schwager A, Lee M, Raff JW, Hyman AA (2005) Aurora A phosphorylation of TACC3/maskin is required for centrosome-dependent microtubule assembly in mitosis. *J Cell Biol* 170: 1047–1055
- Kirilly D, Gu Y, Huang Y, Wu Z, Bashirullah A, Low BC, Kolodkin AL, Wang H, Yu F (2009) A genetic pathway composed of Sox14 and Mical governs severing of dendrites during pruning. *Nat Neurosci* 12: 1497–1505
- Kirilly D, Wong JJ, Lim EK, Wang Y, Zhang H, Wang C, Liao Q, Wang H, Liou YC, Yu F (2011) Intrinsic epigenetic factors cooperate with the steroid hormone ecdysone to govern dendrite pruning in *Drosophila*. *Neuron* 72: 86–100
- Kuo CT, Jan LY, Jan YN (2005) Dendrite-specific remodeling of *Drosophila* sensory neurons requires matrix metalloproteases, ubiquitin-proteasome, and ecdysone signaling. *Proc Natl Acad Sci USA* 102: 15230–15235
- Lee T, Luo L (2001) Mosaic analysis with a repressible cell marker (MARCM) for *Drosophila* neural development. *Trends Neurosci* 24: 251–254
- Lee MJ, Gergely F, Jeffers K, Peak-Chew SY, Raff JW (2001) Msps/XMAP215 interacts with the centrosomal protein D-TACC to regulate microtubule behaviour. *Nat Cell Biol* 3: 643–649
- Lee HH, Jan LY, Jan YN (2009) *Drosophila* IKK-related kinase Ik2 and Katanin p60-like 1 regulate dendrite pruning of sensory neuron during metamorphosis. *Proc Natl Acad Sci USA* 106: 6363–6368
- Li W, Moriwaki T, Tani T, Watanabe T, Kaibuchi K, Goshima G (2012) Reconstitution of dynamic microtubules with *Drosophila* XMAP215, EB1, and Scentin. *J Cell Biol* 199: 849–862
- Loncle N, Williams DW (2012) An interaction screen identifies headcase as a regulator of large-scale pruning. *J Neurosci* 32: 17086–17096
- Lowery LA, Stout A, Faris AE, Ding L, Baird MA, Davidson MW, Danuser G, Van Vactor D (2013) Growth cone-specific functions of XMAP215 in restricting microtubule dynamics and promoting axonal outgrowth. *Neural Dev* 8: 22
- Luo L, O'Leary DD (2005) Axon retraction and degeneration in development and disease. *Annu Rev Neurosci* 28: 127–156
- Maniar TA, Kaplan M, Wang GJ, Shen K, Wei L, Shaw JE, Koushika SP, Bargmann CI (2011) UNC-33 (CRMP) and ankyrin organize microtubules and localize kinesin to polarize axon-dendrite sorting. *Nat Neurosci* 15: 48–56
- Mao CX, Xiong Y, Xiong Z, Wang Q, Zhang YQ, Jin S (2014) Microtubule-severing protein Katanin regulates neuromuscular junction development and dendritic elaboration in *Drosophila*. *Development* 141: 1064–1074
- Martin-Blanco E, Gampel A, Ring J, Virdee K, Kirov N, Tolkovsky AM, Martinez-Arias A (1998) puckered encodes a phosphatase that mediates a feedback loop regulating JNK activity during dorsal closure in *Drosophila*. *Genes Dev* 12: 557–570
- Massaro CM, Pielage J, Davis GW (2009) Molecular mechanisms that enhance synapse stability despite persistent disruption of the spectrin/ankyrin/microtubule cytoskeleton. *J Cell Biol* 187: 101–117
- Matsubara D, Horiuchi SY, Shimono K, Usui T, Uemura T (2011) The seven-pass transmembrane cadherin Flamingo controls dendritic self-avoidance via its binding to a LIM domain protein, Espinas, in *Drosophila* sensory neurons. *Genes Dev* 25: 1982–1996

- Mattie FJ, Stackpole MM, Stone MC, Clippard JR, Rudnick DA, Qiu Y, Tao J, Allender DL, Parmar M, Rolls MM (2010) Directed microtubule growth, +TIPs, and kinesin-2 are required for uniform microtubule polarity in dendrites. *Curr Biol* 20: 2169–2177
- McNally FJ, Vale RD (1993) Identification of katanin, an ATPase that severs and disassembles stable microtubules. *Cell* 75: 419–429
- Mennella V, Rogers GC, Rogers SL, Buster DW, Vale RD, Sharp DJ (2005) Functionally distinct kinesin-13 family members cooperate to regulate microtubule dynamics during interphase. *Nat Cell Biol* 7: 235–245
- Mohan R, Katrukha EA, Doodhi H, Smal I, Meijering E, Kapitein LC, Steinmetz MO, Akhmanova A (2013) End-binding proteins sensitize microtubules to the action of microtubule-targeting agents. *Proc Natl Acad Sci USA* 110: 8900–8905
- Nguyen MM, McCracken CJ, Milner ES, Goetschius DJ, Weiner AT, Long MK, Michael NL, Munro S, Rolls MM (2014) Gamma-tubulin controls neuronal microtubule polarity independently of Golgi outposts. *Mol Biol Cell* 25: 2039–2050
- Nwagbara BU, Faris AE, Bearce EA, Erdogan B, Ebbert PT, Evans MF, Rutherford EL, Enzenbacher TB, Lowery LA (2014) TACC3 is a microtubule plus end-tracking protein that promotes axon elongation and also regulates microtubule plus end dynamics in multiple embryonic cell types. *Mol Biol Cell* 25: 3350–3362
- Ori-McKenney KM, Jan LY, Jan YN (2012) Golgi outposts shape dendrite morphology by functioning as sites of acentrosomal microtubule nucleation in neurons. *Neuron* 76: 921–930
- Port F, Chen HM, Lee T, Bullock SL (2014) Optimized CRISPR/Cas tools for efficient germline and somatic genome engineering in *Drosophila*. *Proc Natl Acad Sci USA* 111: E2967–E2976
- Riccomagno MM, Kolodkin AL (2015) Sculpting neural circuits by axon and dendrite pruning. *Annu Rev Cell Dev Biol* 31: 779–805
- Rolls MM, Satoh D, Clyne PJ, Henner AL, Uemura T, Doe CQ (2007) Polarity and intracellular compartmentalization of *Drosophila* neurons. *Neural Dev* 2: 7
- Satoh D, Sato D, Tsuyama T, Saito M, Ohkura H, Rolls MM, Ishikawa F, Uemura T (2008) Spatial control of branching within dendritic arbors by dynein-dependent transport of Rab5-endosomes. *Nat Cell Biol* 10: 1164–1171
- Schuldiner O, Yaron A (2015) Mechanisms of developmental neurite pruning. *Cell Mol Life Sci* 72: 101–119
- Stepanova T, Slemmer J, Hoogenraad CC, Lansbergen G, Dortland B, De Zeeuw CI, Grosveld F, van Cappellen G, Akhmanova A, Galjart N (2003) Visualization of microtubule growth in cultured neurons via the use of EB3-GFP (end-binding protein 3-green fluorescent protein). *J Neurosci* 23: 2655–2664
- Stewart A, Tsubouchi A, Rolls MM, Tracey WD, Sherwood NT (2012) Katanin p60-like1 promotes microtubule growth and terminal dendrite stability in the larval class IV sensory neurons of *Drosophila*. *J Neurosci* 32: 11631–11642
- Stone MC, Roegiers F, Rolls MM (2008) Microtubules have opposite orientation in axons and dendrites of *Drosophila* neurons. *Mol Biol Cell* 19: 4122–4129
- Stone MC, Albertson RM, Chen L, Rolls MM (2014) Dendrite injury triggers DLK-independent regeneration. *Cell Rep* 6: 247–253
- Tang G, Gudsnek K, Kuo SH, Cotrina ML, Rosoklija G, Sosunov A, Sonders MS, Kanter E, Castagna C, Yamamoto A et al (2014) Loss of mTOR-dependent macroautophagy causes autistic-like synaptic pruning deficits. *Neuron* 83: 1131–1143
- Tao J, Feng C, Rolls MM (2016) The microtubule-severing protein fidgetin acts after dendrite injury to promote their degeneration. *J Cell Sci* 129: 3274–3281
- Tenenbaum CM, Gavis ER (2016) Removal of *Drosophila* muscle tissue from larval fillets for immunofluorescence analysis of sensory neurons and epidermal cells. *J Vis Exp* 117: 54670
- Terman JR, Mao T, Pasterkamp RJ, Yu HH, Kolodkin AL (2002) MICALs, a family of conserved flavoprotein oxidoreductases, function in plexin-mediated axonal repulsion. *Cell* 109: 887–900
- Thakur HC, Singh M, Nagel-Steger L, Kremer J, Prumbaum D, Fansa EK, Ezzahoini H, Nouri K, Gremer L, Abts A et al (2014) The centrosomal adaptor TACC3 and the microtubule polymerase chTOG interact via defined C-terminal subdomains in an Aurora-A kinase-independent manner. *J Biol Chem* 289: 74–88
- Thawani A, Kadzik RS, Petry S (2018) XMAP215 is a microtubule nucleation factor that functions synergistically with the gamma-tubulin ring complex. *Nat Cell Biol* 20: 575–585
- van der Vaart B, Franker MA, Kuijpers M, Hua S, Bouchet BP, Jiang K, Grigoriev I, Hoogenraad CC, Akhmanova A (2012) Microtubule plus-end tracking proteins SLAIN1/2 and ch-TOG promote axonal development. *J Neurosci* 32: 14722–14728
- Wang Y, Zhang H, Shi M, Liou YC, Lu L, Yu F (2017) Sec71 functions as a GEF for the small GTPase Arf1 to govern dendrite pruning of *Drosophila* sensory neurons. *Development* 144: 1851–1862
- Wang Y, Rui M, Tang Q, Bu S, Yu F (2019) Patronin governs minus-end-out orientation of dendritic microtubules to promote dendrite pruning in *Drosophila*. *Elife* 8: e39964
- Williams DW, Truman JW (2005) Cellular mechanisms of dendrite pruning in *Drosophila*: insights from *in vivo* time-lapse of remodeling dendritic arborizing sensory neurons. *Development* 132: 3631–3642
- Witte H, Neukirchen D, Bradke F (2008) Microtubule stabilization specifies initial neuronal polarization. *J Cell Biol* 180: 619–632
- Wong JJ, Li S, Lim EK, Wang Y, Wang C, Zhang H, Kirilly D, Wu C, Liou YC, Wang H et al (2013) A Cullin1-based SCF E3 ubiquitin ligase targets the InR/PI3K/TOR pathway to regulate neuronal pruning. *PLoS Biol* 11: e1001657
- Xiong X, Wang X, Ewanek R, Bhat P, Diantonio A, Collins CA (2010) Protein turnover of the Wallenda/DLK kinase regulates a retrograde response to axonal injury. *J Cell Biol* 191: 211–223
- Yalgin C, Karim MR, Moore AW (2011) Immunohistological labeling of microtubules in sensory neuron dendrites, tracheae, and muscles in the *Drosophila* larva body wall. *J Vis Exp* 57: 3662
- Yalgin C, Ebrahimi S, Delandre C, Yoong LF, Akimoto S, Tran H, Amikura R, Spokony R, Torben-Nielsen B, White KP et al (2015) Centrosomin represses dendrite branching by orienting microtubule nucleation. *Nat Neurosci* 18: 1437–1445
- Yan J, Chao DL, Toba S, Koyasako K, Yasunaga T, Hirotsune S, Shen K (2013) Kinesin-1 regulates dendrite microtubule polarity in *Caenorhabditis elegans*. *Elife* 2: e00133
- Ye B, Zhang Y, Song W, Younger SH, Jan LY, Jan YN (2007) Growing dendrites and axons differ in their reliance on the secretory pathway. *Cell* 130: 717–729
- Yu W, Solowska JM, Qiang L, Karabay A, Baird D, Baas PW (2005) Regulation of microtubule severing by katanin subunits during neuronal development. *J Neurosci* 25: 5573–5583
- Yu F, Schuldiner O (2014) Axon and dendrite pruning in *Drosophila*. *Curr Opin Neurobiol* 27: 192–198
- Zhang H, Wang Y, Wong JJ, Lim KL, Liou YC, Wang H, Yu F (2014) Endocytic pathways downregulate the L1-type cell adhesion molecule neuroglian to promote dendrite pruning in *Drosophila*. *Dev Cell* 30: 463–478
- Zheng Y, Wildonger J, Ye B, Zhang Y, Kita A, Younger SH, Zimmerman S, Jan LY, Jan YN (2008) Dynein is required for polarized dendritic transport and uniform microtubule orientation in axons. *Nat Cell Biol* 10: 1172–1180